



# Understanding the influence of ENSO patterns on drought over southern Africa using SPEEDY

Michelle Gore<sup>1</sup> · Babatunde J. Abiodun<sup>2</sup> · Fred Kucharski<sup>3</sup>

Received: 5 February 2019 / Accepted: 25 September 2019  
© Springer-Verlag GmbH Germany, part of Springer Nature 2019

## Abstract

The El Niño Southern Oscillation (ENSO) is a major driver of southern Africa drought, but the nonlinearity of ENSO variation inhibits accurate drought prediction. While studies have identified multiple sea surface temperature (SST) patterns associated with ENSO, most drought predictions over southern Africa are still based on only two patterns. This study examines the relationship between southern Africa droughts and eight ENSO SST patterns using SPEEDY. The capability of SPEEDY in reproducing southern Africa climate was evaluated by comparing historical simulations (1979–2008) with observation. To understand the influence of ENSO SST patterns on southern Africa drought, multi-ensemble simulations were forced with SSTs of each pattern, and the impacts on the Standardized Precipitation Evapotranspiration Index (SPEI) and the associated atmospheric dynamics were analysed. The results show that SPEEDY generally captures the temporal and spatial distribution of climate variables over southern Africa well, although with a warm and wet bias. However, the results are comparable with those from more complex atmospheric models. In agreement with previous studies, the results show that El Niño (La Niña) conditions weaken (strengthen) the Walker circulation, causing drier (wetter) conditions over parts of southern Africa. However, the results show that differences in the El Niño conditions alter the moisture flux circulation over southern Africa, thereby influencing the spatial pattern and intensity of drought over the region. The same is true of the La Niña conditions. Hence, this study shows that accounting for the differences in El Niño (or La Niña) conditions may improve drought predictions in southern Africa.

**Keywords** Droughts · Southern Africa · ENSO · Teleconnections · SPEEDY

## 1 Introduction

In southern Africa, the El Niño Southern Oscillation (ENSO) is generally considered to be the dominant mode of interannual climate variability with the greatest impact on summer rainfall, often resulting in drought (Nicholson

and Entekhabi 1987; Lindesay 1988; Nicholson and Kim 1997; Reason et al. 2000; Cook 2001; Reason and Jagadeesha 2005). ENSO is an ocean–atmosphere phenomenon that consists of large-scale warming (El Niño) or cooling (La Niña) of the equatorial Pacific sea surface temperatures (SST). These SST anomalies affect the lower tropospheric pressure fields, alter the Walker circulation, and influence moisture transport and precipitation globally (Larkin and Harrison 2005; Kao and Yu 2009; Chretien et al. 2015; Hoell et al. 2015). Although the influence of ENSO on southern Africa climate has been well documented, the impacts are highly variable as SST anomalies in the tropical Pacific Ocean can vary considerably between ENSO events. These anomalies are compounded by different modes of variability within the Indian Ocean (e.g. Indian Ocean Dipole and Subtropical Indian Ocean Dipole) and Atlantic Ocean (e.g. Benguela Niño), which have also been shown to modulate regional circulation and rainfall over southern Africa (Shannon et al. 1986; Goddard and Graham 1999; Saji et al. 1999;

**Electronic supplementary material** The online version of this article (<https://doi.org/10.1007/s00382-019-05002-w>) contains supplementary material, which is available to authorized users.

✉ Michelle Gore  
michegore@gmail.com

<sup>1</sup> Department of Environmental and Geographical Science, University of Cape Town, Cape Town, South Africa

<sup>2</sup> Climate System Analysis Group, Department of Environmental and Geographical Science, University of Cape Town, Cape Town, South Africa

<sup>3</sup> Earth System Physics Section, Abdus Salam International Centre for Theoretical Physics, Trieste, Italy

Behera and Yamagata 2001; Reason 2001; Rouault et al. 2003). In order to better understand the nonlinear impacts of ENSO on southern Africa climate, this study will investigate the relationship between eight global ENSO SST patterns (described by Johnson 2013 and Hoell et al. 2015) and southern Africa drought.

Drought is one of the most devastating natural hazards with severe impacts on the socio-economic sector, especially when the population depends on rain-fed agriculture. Drought usually results in crop failures and livestock death which can lead to food shortages, economic loss, and high inflation rates (Wilhite 2000; Calow et al. 2010; Hayes et al. 2012). A long-term hydrological drought can also cause water scarcity, thereby inducing widespread waterborne diseases because of reliance on unsafe water sources. In addition, drought is a threat to water management, power availability, and ecosystem health (Wilhite 2000; Calow et al. 2010; Davis-Reddy and Vincent 2017). Southern Africa is especially susceptible to widespread drought because of its semi-arid climate, high rainfall variability, and the complex topography of the sub-continent (Mason and Joubert 1997; Goddard and Graham 1999; Yuan et al. 2014). For example, in 1991/1992, an extensive drought severely affected over 90% of inland dams due to a significant drop in the summer rainfall. This resulted in the destruction of many crops and outbreaks of cholera and dysentery affecting the population (Meque and Abiodun 2015; Ujeneza and Abiodun 2015). Rouault and Richard (2005) investigated the spatio-temporal characteristics of drought throughout the twentieth century in southern Africa and found that over 66% of severe droughts could be attributed to ENSO. It has also been observed that the influence of ENSO on southern Africa climate has strengthened since the 1970s (Rouault and Richard 2005) and there is concern that the intensity and severity of southern Africa droughts may increase in the future due to ongoing global warming (Shongwe et al. 2009). Therefore, there is a need for more studies to investigate the relationship between southern Africa droughts and ENSO teleconnections in an effort to improve drought predictions and reduce drought impacts on human activities in the region.

Most studies agree that El Niño (La Niña) typically reduces (intensifies) precipitation over the southeastern region of Africa, resulting in dry (wet) conditions, while increasing (decreasing) precipitation over the northeastern tropical region (Tyson and Preston-Whyte 2000; Ashok et al. 2007; Davis 2011; Hoell et al. 2015; Yuan et al. 2014; Meque and Abiodun 2015). These precipitation anomalies can be attributed to changes in various synoptic-scale atmospheric features, such as the Angola low (Reason and Jagadheesha 2005), Walker Circulation (Lindesay 1988), tropical cyclones (Ash and Matyas 2012), South Indian Convergence Zone (SICZ) and tropical temperate troughs

(TTT; Cook 2000, 2001; Meque and Abiodun 2015). Nevertheless, many studies identify that the relationship between ENSO and southern Africa rainfall is nonlinear (Tyson and Preston-Whyte 2000; Reason and Jagadheesha 2005; Fauchereau et al. 2009; Yuan et al. 2014). There is high variability in the spatial extent, timing and intensity of the impacts. For example, the strong El Niño event of 1997, which had notable impacts around the globe, had little to no impacts on rainfall in southern Africa (Tyson and Preston-Whyte 2000; Hoell et al. 2017). This nonlinear relationship can be explained by internal variability of ENSO SST anomalies within the Pacific Ocean, creating different patterns or ‘flavours’ (Kao and Yu 2009). The need to understand the influence of different ENSO patterns on regional climate led Johnson (2013) to identify eight ENSO SST patterns over the Pacific Ocean (i.e. four El Niño conditions and four La Niña conditions). In addition, some studies have highlighted the role of the other ocean basins and modes of variability in southern Africa climate (e.g. Goddard and Graham 1999; Behera and Yamagata 2001; Reason 2001; Rouault et al. 2003). For instance, Reason and Jagadheesha (2005) attribute the lack of response to the 1997 strong El Niño, to a positive IOD and warm SST off the west coast of southern Africa. Therefore, to further the work of Johnson (2013), Hoell et al. (2015) examined the influence of each ENSO pattern on tropical SST in the Atlantic Ocean and Indian Ocean, global atmospheric circulation, and southern Africa precipitation during the period 1950–2010. The study clearly showed that the four El Niño conditions produce different rainfall patterns over southern Africa; and the same is true for the four La Niña conditions.

While Hoell et al. (2015) focus their study on precipitation anomalies, the main factor when considering drought, studies have shown that other climate variables (e.g. temperature, wind, relative humidity, precipitation duration, intensity and onset) can also influence the frequency and severity of drought (Mishra and Singh 2010; Vicente-Serrano et al. 2010; Trambauer et al. 2014). Temperature can be particularly influential to drought severity as it plays a crucial role in atmospheric evaporative demand. Additionally, studies (e.g. Meque and Abiodun 2015; Ujeneza and Abiodun 2015; Manatsa et al. 2017) have shown that ENSO influences both precipitation and temperature over southern Africa. Meque and Abiodun (2015) even found that ENSO has a higher correlation with temperature than with rainfall over the subtropical part of southern Africa. Hence, the use of only precipitation could underestimate the impact of ENSO patterns on droughts over southern Africa. To address this, the present study intends to investigate the link between ENSO SST patterns and southern Africa drought by using the Standardized Precipitation Evapotranspiration Index (SPEI) to quantify drought. SPEI, which is based on the climate water balance, accounts for the influence of both

precipitation and potential evapotranspiration in drought quantifications (Vicente-Serrano et al. 2010; Meque and Abiodun 2015; Ujeneza and Abiodun 2015; Manatsa et al. 2017; Abiodun et al. 2019).

This study aims to build on the observational evidence presented by Hoell et al. (2015) by using an ensemble modelling framework. This will enable a more robust result by creating multiple instances of each ENSO pattern, which observation data does not provide as the number of events for each ENSO pattern is small. Such simulations will improve the distinction between the forced and internal variability, and at the same time reduce the uncertainty of the signal (Bracco et al. 2004; Kucharski et al. 2013a). Studies generally approach ensemble simulations one of two ways: either they use a multi-model approach (e.g. Dieppois et al. 2015; Meque and Abiodun 2015) or they perform multiple simulations using the same model with slight perturbations in the initial conditions (e.g. Dogar et al. 2017). Unfortunately, complex AGCMs are usually computationally expensive and have limited availability. To perform such multi-ensemble simulations would require massive computational resources that are not available to many institutions in developing countries like South Africa. Using a simple AGCM (like SPEEDY) for such sensitivity experiments is a good alternative. That is the approach used in the present study. SPEEDY (Simplified Parameterizations, primitivE-Equation DYnamics) is a model of intermediate complexity that simulates global atmospheric circulation well (see Molteni 2003; Kucharski et al. 2006). SPEEDY has been successfully used to simulate large-scale features like the Indian and African monsoon (e.g. Bracco et al. 2007; Kucharski et al. 2009, 2011; Feudale and Kucharski 2013), East Africa rainfall variability (e.g. Bahaga et al. 2015) and ENSO studies (e.g. Yadav et al. 2010; Bulić and Kucharski 2012; Dogar et al. 2017). However, the capability of SPEEDY in simulating southern Africa rainfall has not been tested, and that is a focus in the present study. Previous studies (e.g. Zeng et al. 1999; Wang and Eltahir 2000a, b; Zeng and Yoon 2009; Kucharski et al. 2013b) have also identified that climate variability can also be enhanced by vegetation interactions (e.g. evapotranspiration, albedo, roughness and leaf area index) which modify the atmospheric energy and water balance. While many studies have shown vegetation feedbacks to be important in the Sahel region (e.g. Zeng et al. 1999; Wang and Eltahir 2000a, b; Kucharski et al. 2013b), their role is unclear in southern Africa climate. Naik and Abiodun (2016) have shown that the southern Africa climate is sensitive to vegetation feedbacks, however Nicholson (2000) disagrees, stating that land–atmosphere feedbacks are not present in the subcontinent. Therefore, this study will also assess the influence of coupling SPEEDY with a dynamic vegetation model.

Hence, the aim of this study is to examine the relationship between southern Africa droughts and patterns of ENSO using SPEEDY. The study evaluates the capability of SPEEDY in simulating the southern Africa climate and then applies the model to perform a series of sensitivity simulations with different global SST patterns to investigate the link between southern Africa droughts and ENSO patterns. The paper is structured as follows. Section 2 describes the data and model used in the study as well as the experiment design. Section 3 presents the results and Sect. 4 gives a summary and discussion.

## 2 Data and methodology

### 2.1 Model description

The model used in this study is the ICTPAGCM (version 41.5), known as SPEEDY (Simplified Parameterizations, primitivE-Equation DYnamics), developed at the Abdus Salam International Center for Theoretical Physics (ICTP) (see Molteni 2003; Kucharski et al. 2006). It is an intermediate complexity model based on a hydrostatic spectral dynamical core (see Held and Suarez 1994) and uses the vorticity-divergence form described by Bourke (1974). It has several simplified physical parameterization schemes including convection, large-scale condensation, vertical diffusion, short and longwave radiation and surface fluxes of momentum, heat and moisture. SPEEDY uses a mass flux scheme to represent convection processes, which is activated by the presence of conditional instability, and boundary layer fluxes are determined by stability-dependent bulk formulae. Additionally, SPEEDY is coupled with a simple one-layer thermodynamic model to determine land and ice temperature anomalies. Despite the simplified parameterizations, SPEEDY has reasonable performance and has been successfully implemented in a wide variety of climate research, including ENSO studies (e.g. Yadav et al. 2010; Bulić and Kucharski 2012; Dogar et al. 2017). Its computational efficiency and flexibility make it an ideal tool for this study. A more detailed description of SPEEDY is provided by Molteni (2003) and Kucharski et al. (2006) and information about the model versions, performance, users and access can be found at <http://users.ictp.it/~kucharsk/speedy-net.html>.

### 2.2 Data

SPEEDY simulations were conducted at T63 spectral truncation resolution ( $\sim 1.875^\circ \times 1.875^\circ$ ) with 8 vertical levels, using monthly mean climatological SST data derived from ERA-Interim over the period 1979–2008 and observed SST anomalies from the Met Office Hadley Centre (HadISST). Studies (e.g. Zeng et al. 1999; Kucharski et al. 2013b; Li

et al. 2018) have shown that vegetation dynamics (e.g. evapotranspiration, albedo, roughness and leaf area index) can influence the climate by modifying the atmospheric energy and water balance. Therefore, it is important to incorporate vegetation feedbacks to enable two-way vegetation-climate interactions. This study coupled SPEEDY with two different land-surface schemes: a dynamic vegetation scheme (SPEEDY-DV) and a non-dynamic vegetation scheme (SPEEDY-NDV). The SPEEDY-DV simulations coupled SPEEDY with the dynamic vegetation model VEGAS (Vegetation–Global–Atmosphere–Soil) which enabled fully interactive vegetation. VEGAS simulates the dynamics of vegetation growth and competition among four plant functional types (broadleaf tree, needleleaf tree, cold grass and warm grass) with different photosynthetic pathways (Kucharski et al. 2013b; Li et al. 2018). The SPEEDY-NDV simulations prescribed climatological vegetation cover and only coupled SPEEDY with land temperature and soil moisture changes. An extended force-restore type approach is used to determine sea-ice temperatures in the coupled ice model in SPEEDY. However, SPEEDY is not coupled with the slab ocean model as SST anomalies are prescribed in the experimental design.

Observed and simulated monthly climate data were used to evaluate the performance of the SPEEDY simulations. The observed data used in this study is from the Climate Research Unit (CRU). It consists of monthly climate estimates which have been re-gridded to a  $0.5^\circ \times 0.5^\circ$  spatial resolution. Monthly climate data from the National Center for Atmospheric Research (NCAR) Community Atmospheric Model version 5 (CAM5, spatial resolution  $\sim 1^\circ \times 1^\circ$ ) and the UK Met Office Hadley Centre Global Environment Model version 3 (HadGEM3, spatial resolution  $\sim 0.556^\circ \times 0.833^\circ$ ) were also included in the model evaluation. The CAM5 (see Angéllil et al. 2017; Stone et al. 2018) and HadGEM3 (see Christidis et al. 2013; Ciavarella et al. 2018) simulations are from the Climate of the 20th Century Plus Detection and Attribution project (C20C + D&A) undertaken by the World Climate Research Program's CLIVAR. These historical ensemble simulations ("All-Hist") are CMIP5-style simulations forced with prescribed radiative forcing, SSTs and sea ice conditions (see Stone et al. 2019 for detailed experimental design). For consistency, all simulated data (SPEEDY, CAM5 and HadGEM3) was re-gridded to the same resolution as CRU ( $0.5^\circ \times 0.5^\circ$ ) and only one ensemble member was used from CAM5 and HadGEM3.

### 2.3 Model evaluation

The capability of SPEEDY in simulating the climate of southern Africa ( $5^\circ\text{E}$ – $52^\circ\text{E}$ ;  $0^\circ\text{S}$ – $40^\circ\text{S}$ ) was evaluated over a historical period of 30 years (1979–2008). Throughout the model evaluation, we compared the SPEEDY

simulations (SPEEDY-DV and SPEEDY-NDV) with estimates of observed conditions from CRU using statistical analysis. The inclusion of CAM5 and HadGEM3 served as a benchmark to compare the error of SPEEDY with the error of more complex GCMs with higher resolution. Analysis of the seasonal and spatial climate variability was done to evaluate the performance of SPEEDY over three distinct areas—tropical ( $30^\circ\text{E}$ – $40^\circ\text{E}$ ;  $0.5^\circ\text{S}$ – $8^\circ\text{S}$ ), subtropical ( $25^\circ\text{E}$ – $33^\circ\text{E}$ ;  $18^\circ\text{S}$ – $26^\circ\text{S}$ ) and semi-arid ( $15^\circ\text{E}$ – $23^\circ\text{E}$ ;  $22^\circ\text{S}$ – $30^\circ\text{S}$ ) (Fig. 1). This study focused on the austral summer season (December–February, DJF) as this is the main rainy season for the majority of southern Africa (Tyson and Preston-Whyte 2000; Davis 2011). The climate variables which were analysed include temperature (mean, maximum and minimum), precipitation, potential evapotranspiration (PET) and the climate moisture balance (CMB). CMB is a measure of the atmospheric water budget by considering the difference between supply (e.g. precipitation) and demand (e.g. PET), taking into account the influence of many variables, including precipitation and temperature. There are various formulations to calculate PET, including Thornthwaite (based on mean temperature), Hargreaves (based on minimum and maximum temperature), and Penman–Monteith (based on air temperature, solar radiation, relative humidity and wind speed) methods. In this paper PET will be calculated using the Hargreaves method as it is a less data-intensive approach, but still provides reliable evapotranspiration estimates, including in semi-arid regions such as southern Africa (Hargreaves and Allen 2003).

Various drought indices have been developed to quantify drought characteristics (such as duration, spatial extent and intensity), which are useful for monitoring and management of drought (Mishra and Singh 2010; Vicente-Serrano et al. 2010; Hayes et al. 2012). SPEI combines the strengths of the Palmer Drought Severity Index and the Standardized Precipitation Index, showing sensitivity to evaporative demand as well as multi-temporal capabilities (Meque and Abiodun 2015; Ujeneza and Abiodun 2015). Therefore, SPEI is used in this study to identify meteorological drought (3-month timescale). SPEI is obtained by fitting a three parameter probability distribution to the CMB from which the standardized deviation of a period is measured against the long term mean (see Vicente-Serrano et al. 2010 for detailed equations). This provides an indication of the intensity of dryness ranging from  $\leq -2$  for extreme drought to  $\geq 2$  for extreme wet conditions. SPEI was computed at a 3-month scale over southern Africa using the SPEI library available in R software (Beguería and Vicente-Serrano 2013). A log-logistic probability distribution was used, as recommended by Vicente-Serrano et al. (2010), using unbiased Probability Weighted Moments for parameter fitting as suggested by Beguería et al. (2014).

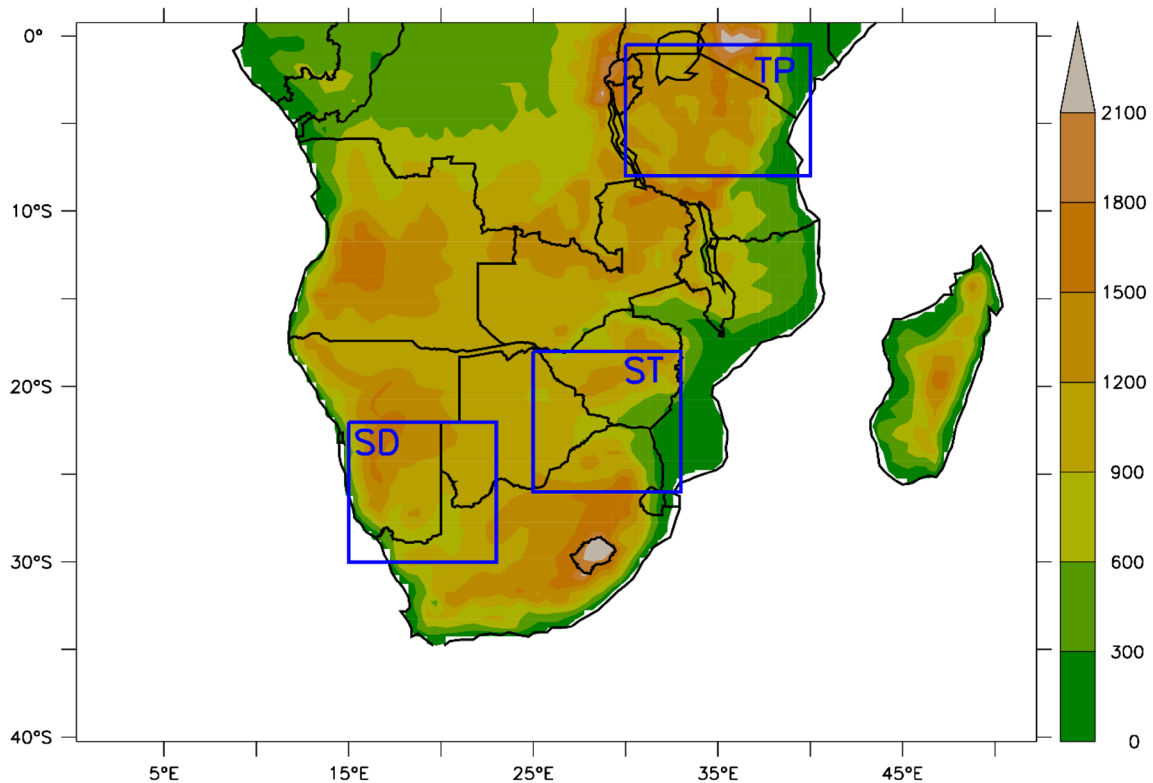


**Fig. 1** The study domain showing southern African topography and the selected three areas for model evaluation. The designated areas are semi-arid (SD), subtropical (ST) and tropical (TP)

In order to determine if SPEEDY could capture the fundamental influence of ENSO on summer climate in southern Africa, the temporal correlation was calculated between various climate variables (SPEI, precipitation and PET) and the Niño 3.4 index (available from ESRL/NOAA). The Niño 3.4 index is based on monthly averages of SST anomalies across the tropical Pacific Ocean ( $5^{\circ}\text{N}$ – $5^{\circ}\text{S}$ ;  $170^{\circ}\text{W}$ – $120^{\circ}\text{W}$ ), where positive values indicate warm El Niño phases and negative values indicate cool La Niña phases.

## 2.4 Experimental design and methods

This study used eight ENSO SST patterns previously identified by Johnson (2013) and Hoell et al. (2015) through self-organizing map analysis (Fig. 2). They consist of four El Niño conditions (EN1–EN4) and four La Niña conditions (LN1–LN4) which are statistically distinct in terms of the magnitude and position of the associated SST anomalies in the tropical Pacific Ocean. Johnson (2013) also identified the years in which each ENSO pattern occurred for the period 1950–2011. The global SST composites for each ENSO pattern were created by averaging the HadISST data for the years in which that pattern occurred (as identified by Johnson 2013). There are some notable differences between the ENSO SST patterns which are discussed in detail in Hoell

et al. (2015). The El Niño SST patterns (EN1–EN4) show a significant warm anomaly in the tropical Pacific Ocean, with increasing size and intensity from EN1 to EN4. The warm SST anomaly has a more central position during EN1, EN2 and EN3, characteristic of Central Pacific ENSO (also known as ‘dateline ENSO’, ‘warm pool ENSO’ or ‘ENSO Modoki’), whereas EN4 is characteristic of Eastern Pacific ENSO (also known as ‘canonical ENSO’) with the warm anomaly extending across the eastern Pacific Ocean (Hoell et al. 2015). The western Pacific Ocean is characterized by significant cool SST anomalies during EN1, EN3 and EN4. EN1 also features cool SST anomalies in the Indian Ocean and tropical Atlantic Ocean, whilst EN3 and EN4 display significant warm SST anomalies in these ocean basins. The warm Indian Ocean SST anomalies in EN4 are characteristic of a positive Indian Ocean dipole. EN2 shows minimal SST anomalies in the Atlantic Ocean, Indian Ocean and western Pacific Ocean (Hoell et al. 2015). The La Niña SST patterns (LN1–LN4) are characterized by significant cool SST anomalies across the central and eastern Pacific Ocean, with decreasing size from LN1 to LN4. LN1 and LN2 are classified as Eastern Pacific ENSO events, while LN3 and LN4 are classified as Central Pacific ENSO events (Hoell et al. 2015). Significant warm SST anomalies are present in the western Pacific Ocean, tropical Atlantic Ocean as well as parts of the Indian Ocean during LN3 and LN4,

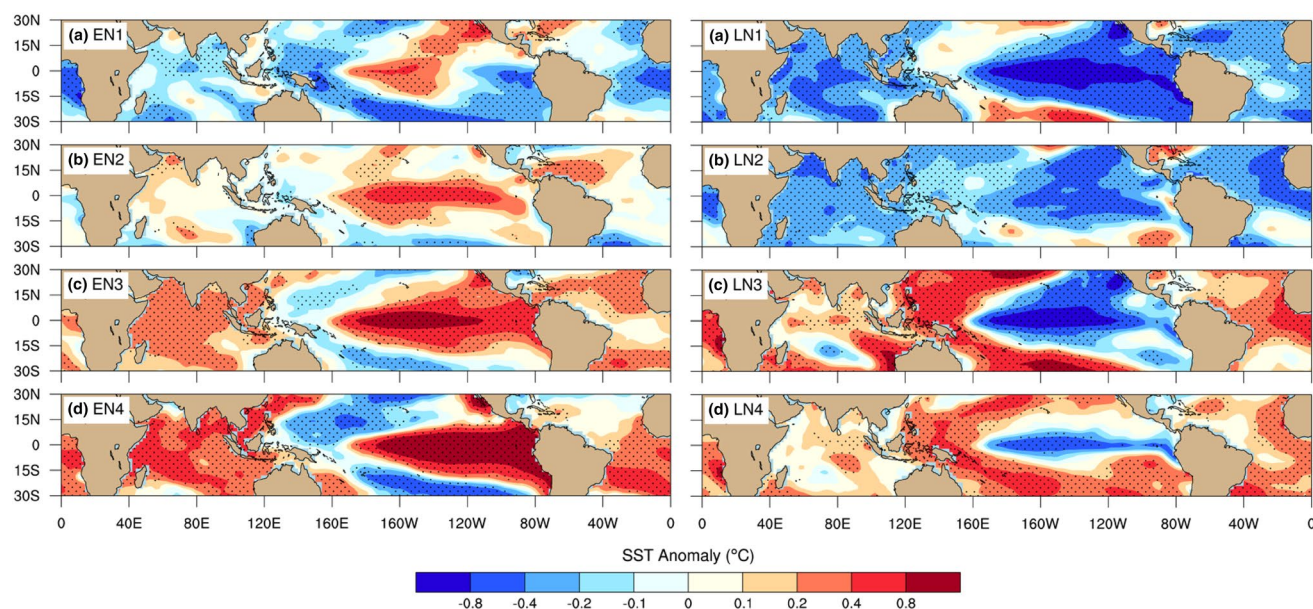


**Fig. 2** Composite SST anomalies (°C) for El Niño (EN1–EN4) and La Niña (LN1–LN4) conditions during austral summer 1950–2010. Stippling indicates anomalies significant at  $p < 0.05$  (source: Hoell et al. 2015)

with LN3 featuring a significant negative Indian Ocean Dipole. In contrast, LN1 and LN2 feature cool SST anomalies across the Atlantic Ocean, Indian Ocean and western Pacific Ocean, except for the western Pacific Ocean in LN1 which shows no significant SST anomalies.

In this study, eight sensitivity experiments were conducted—one for each ENSO SST pattern. In each case, SPEEDY was forced with the composite global SST anomalies associated with that pattern. Each experiment consisted of a 50-member ensemble with perturbations in the start date. We simulated an 18-month period (July to the following December) for each ensemble member whereby the ENSO anomaly occurred during the interim DJF period, which was the focus of our analysis. Through the evaluation it was seen that the simulation with the non-dynamic vegetation scheme performed better over southern Africa and was therefore used in these sensitivity experiments. In order to investigate the link between southern Africa drought and the ENSO patterns, SPEI and the atmospheric dynamics were analysed. This analysis included anomalies in velocity potential, eddy stream function, horizontal winds and integrated moisture flux with statistical significance determined through a Student  $t$  test (99th percentile).

### 3 Results and discussion

#### 3.1 Model evaluation

In general, SPEEDY captures the annual cycle of the southern Africa climate well (Fig. 3). As in CRU observation, the model simulates a warm wet summer season (December, January and February) and a cold dry winter season (June, July, August). This is characteristic of the three selected areas, although the simulated annual cycle is about 1 month earlier than observed, as evident in temperature (Fig. 3a, b, d, e) and precipitation (Fig. 3j, k, l) cycles. In the tropical (TP) area, SPEEDY credibly simulates observed temperatures, which show low annual variability, as well as a bimodal rainfall pattern, which is driven by the seasonal movement of the Intertropical Convergence Zone (ITCZ) that controls the seasonal rainfall over most parts of southern Africa. In agreement with CRU, SPEEDY shows that the tropical area experiences its first rainy season in September to November (during the southward progression of the ITCZ) and its second rainy season in February to April (during the northward retreat

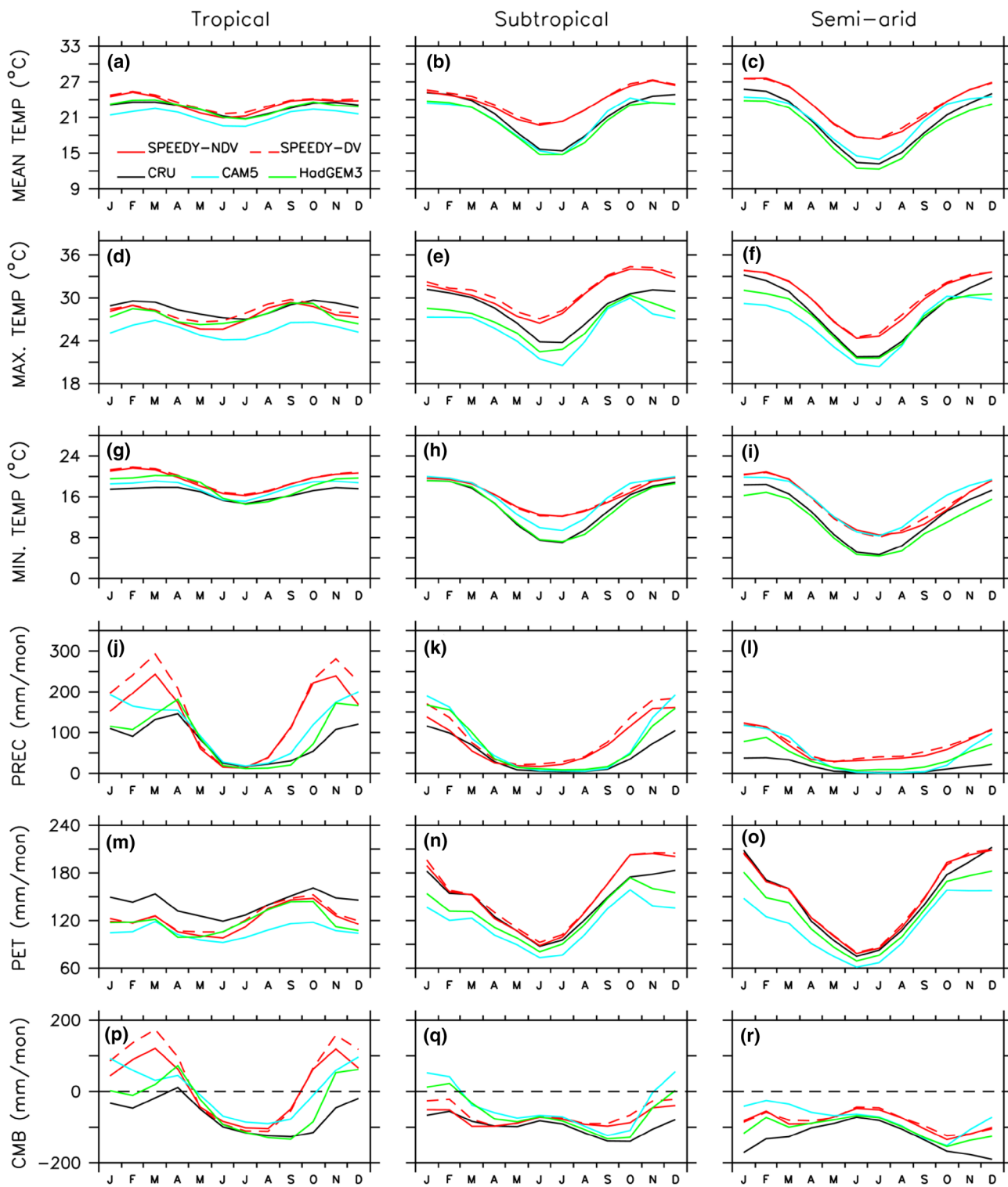


**Fig. 3** The annual cycle of temperature (mean, max and min), precipitation (prec), potential evapotranspiration (PET) and climate moisture balance (CMB) over the three selected areas: semi-arid (SD), subtropical (ST) and tropical (TP) in southern Africa (1979–2008),

as observed by CRU and simulated by SPEEDY (dynamic and non-dynamic vegetation versions: SPEEDY\_DV and SPEEDY\_NDV) and other more complex GCMs (HadGEM3 and CAM5)

of ITCZ). The model also reproduces the low precipitation over the semi-arid area (relative to the other two areas), caused by a lack of moisture in the atmosphere due to the nearby cold Benguela current and dry continental winds.

Nevertheless, there are some noticeable biases in the seasonal cycle produced by SPEEDY. Generally, the model produces a warm and wet bias across the region (Fig. 3). In the subtropical and semi-arid areas, the warm bias varies throughout the year (Fig. 3b, c, e, f, h, i), typically showing the least bias in the summer months ( $\sim 0\text{--}2\text{ }^{\circ}\text{C}$ ) and the highest bias in the winter months ( $\sim 3\text{--}5\text{ }^{\circ}\text{C}$ ). On the other hand, SPEEDY simulates minimal temperature bias in the tropical area (Fig. 3a, d, g). In terms of precipitation, the subtropical area shows maximum precipitation bias during spring ( $\sim 100\text{ mm/month}$ ; Fig. 3k), whilst the semi-arid area shows precipitation bias throughout the year ( $30\text{--}100\text{ mm/month}$ ; Fig. 3l), reaching a maximum in the summer (DJF). However, the tropical area shows the biggest precipitation bias, particularly during the two rainy seasons (September–November and February–March) for which SPEEDY simulates more than double that of CRU observed precipitation ( $100\text{--}180\text{ mm/month}$ ; Fig. 3j). SPEEDY simulates PET relatively well in both the subtropical and semi-arid areas, showing notably less error than the CAM5 and HadGEM3 simulations. Nevertheless, in the tropical area SPEEDY underestimates PET, but this is not dissimilar to the more complex models. The simulated SPEEDY CMB reflects the above analysis by a shift in the climatology of 1 month and overestimation of the CMB due to high simulated values of precipitation. However, these results are similar if not better than the complex models (CAM5 and HadGEM3) in the subtropical and semi-arid areas during the summer. The biases in SPEEDY simulations could be due to the coarse resolution, simplified parameterization schemes or increased sensitivity to orographic features. However, the error is comparable to more complex models and when considering the computational efficiency and flexibility of SPEEDY, it has reasonable performance.

The performance of SPEEDY depends upon the vegetation scheme used. While the simulation with dynamic vegetation (SPEEDY-DV) and the one without dynamic vegetation (SPEEDY-NDV) show similar performance across the three selected areas, SPEEDY-NDV performs better than SPEEDY-DV in most instances, especially in the tropical and subtropical areas (Fig. 3). For instance, SPEEDY-NDV shows less bias than SPEEDY-DV in simulating summer precipitation in the tropical area ( $\sim 50\text{ mm/month}$ ; Fig. 3j), summer and autumn temperatures in the subtropical area ( $1\text{ }^{\circ}\text{C}$ ; Fig. 3e), and winter temperatures in the semi-arid area ( $1\text{ }^{\circ}\text{C}$ ; Fig. 3f, i). However, SPEEDY-DV does feature a better performance than

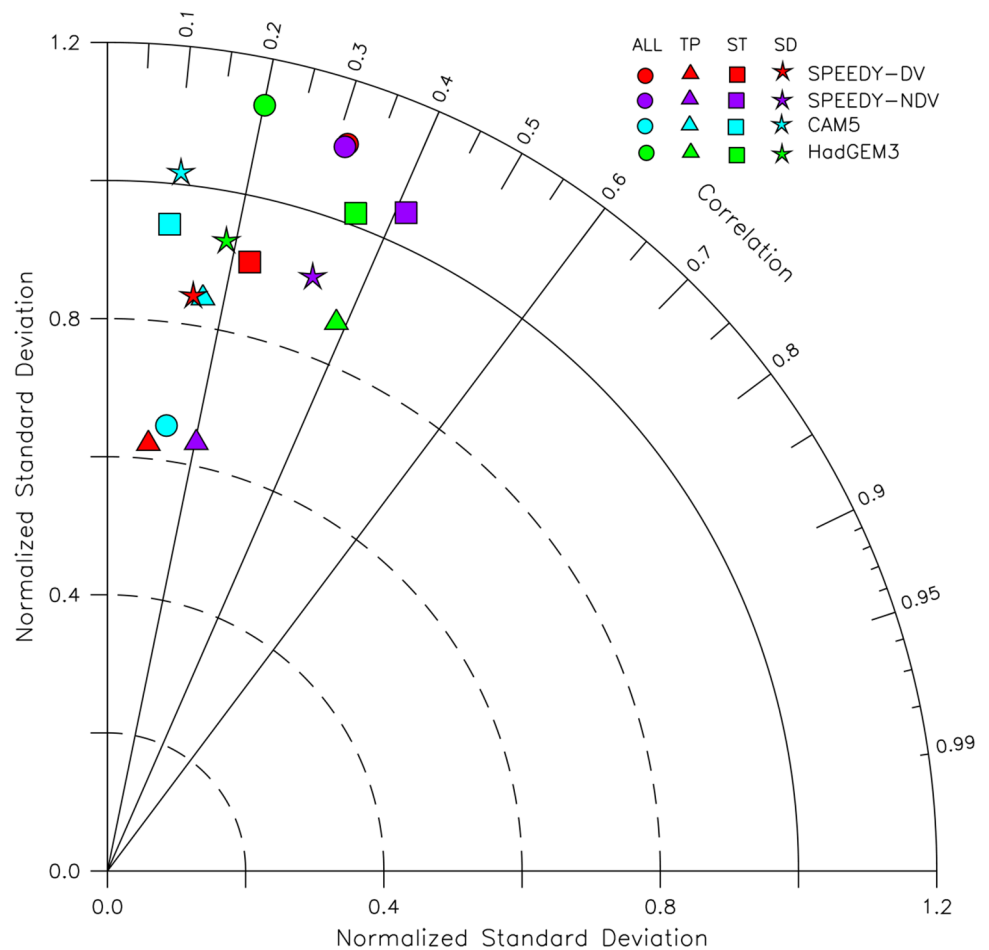
SPEEDY-NDV in reproducing maximum temperature in the tropical area ( $1\text{ }^{\circ}\text{C}$ ; Fig. 3d). Overall, SPEEDY performs better without the dynamic vegetation scheme. This implies that the implementation of dynamic vegetation in SPEEDY does not improve the performance of the model in southern Africa. This contradicts theory which implies that the dynamic vegetation scheme should perform better than static vegetation (Strengers et al. 2010; Li et al. 2018), as the southern Africa climate is sensitive to changes in vegetation (Naik and Abiodun 2016).

SPEEDY captures the interannual variability of summer SPEI with varied capability across regions in southern Africa (Fig. 4). The model features its worst performance in the tropical area with correlation as low as 0.1 and 0.2 (SPEEDY-DV and SPEEDY-NDV, respectively) and a low normalized standard deviation of  $\sim 0.63$  (for both SPEEDY-DV and SPEEDY-NDV). The performance is notably better in the subtropical area with correlation ranging between 0.2 and 0.4. SPEEDY manages to capture most of the variation with high normalized standard deviation (SPEEDY-DV =  $\sim 0.9$  and SPEEDY-NDV =  $\sim 1.05$ ). SPEEDY has average performance in the semi-arid area with correlation between 0.1 and 0.3 for SPEEDY-DV and SPEEDY-NDV, respectively. It has less variability than CRU observation, with normalized standard deviations of  $\sim 0.85$  and  $\sim 0.9$ . Overall the correlations are low, but the results, particularly the SPEEDY-NDV simulation, are comparable to the more complex models, CAM5 and HadGEM3.

SPEEDY generally captures the observed impact of tropical Pacific ENSO SST anomalies on southern Africa climate. As Fig. 5 shows, a positive (negative) Niño 3.4 Index is associated with negative (positive) SPEI, low (high) precipitation and high (low) evapotranspiration, which is characteristic of El Niño (La Niña) and drought (heavy rainfall) in the region. SPEEDY manages to simulate a reasonable representation of this relationship ( $r=0.2\text{--}0.5$ ), nevertheless, there are some biases. These biases are particularly noticeable in the equatorial region and typically consist of a weaker and sometimes opposite correlation being simulated across all three variables (SPEI, PREC and PET). However, the more complex models, CAM5 and HadGEM3, show similar biases and are even bigger in some cases (e.g. CAM5). SPEEDY-NDV generally has less bias than SPEEDY-DV, particularly when correlating Niño 3.4 and SPEI. This is reflected in the spatial correlation where SPEEDY-NDV performs significantly better ( $r=0.5$  and  $r=-0.2$  respectively). SPEEDY-NDV also has better correlation than CAM5, however falls short when compared to the more complex HadGEM3 model.

Further model evaluation is available in supplementary material.

**Fig. 4** Taylor diagram for comparing the observed (CRU) and simulated (SPEEDY-DV, SPEEDY-NDV, CAM5 and HadGEM3) 3-month DJF SPEI over southern Africa, the tropical area (TP), subtropical area (ST) and semi-arid area (SD) from 1979–2008



## 3.2 Sensitivity experiments

### 3.2.1 Drought and atmospheric dynamics associated with El Niño conditions

The spatial pattern and intensity of SPEI drought varies between the El Niño conditions (Fig. 6). EN1 and EN2 (Fig. 6a, b) show SPEI drought in the equatorial area, with significant values (99th percentile) over Angola and Tanzania. This contradicts some previous studies (Tyson and Preston-Whyte 2000; Cook 2001; Hoell et al. 2015) that attributed El Niño conditions with a wet anomaly in the eastern equatorial region. On the other hand, EN3 and EN4 (Fig. 6c, d) show significant SPEI drought condition along the south west of the region, as well as increased drought across central Mozambique and Madagascar. All the El Niño SST conditions show a similar positive SPEI across Botswana and north eastern South Africa, however, these wet conditions are not seen in the results of Hoell et al. (2015), except in EN1. This discrepancy may be a result of the precipitation bias in the SPEEDY simulation, as shown in Fig. 3.

The ensemble spreads of the different El Niño conditions have similar distributions, however there are some notable

differences across the different areas (Fig. 6). In the tropical area there is relatively strong agreement within the ensemble spread, where at least 75% of the ensembles have a negative SPEI for EN1, EN2 and EN3 (Fig. 6). However, this contradicts the literature (Tyson and Preston-Whyte 2000; Hoell et al. 2015) that shows a wet anomaly in this area during El Niño phases. This is also seen in CRU observation which typically shows positive SPEI values. Despite this, CRU observation generally falls within the upper quartile of the ensemble spread. The signal of EN4 in the tropical area remains uncertain. In the subtropical area, most of the ensembles (> 50%) have a positive SPEI for EN1, EN2 and EN3, which is unexpected as drought typically occurs in this area during El Niño phases (Tyson and Preston-Whyte 2000; Hoell et al. 2015). As previously mentioned, this is likely due to the SPEEDY precipitation bias. CRU observation highlights this as well, with most of the observed SPEI falling within the lower two quartiles and below. However, this is not the case for EN1 which only shows positive values for observed SPEI. The semi-arid area shows the biggest ensemble spread and the most uncertainty in the signal. Only EN4 shows some certainty with 75% of the ensembles below zero. The model simulation for this area also

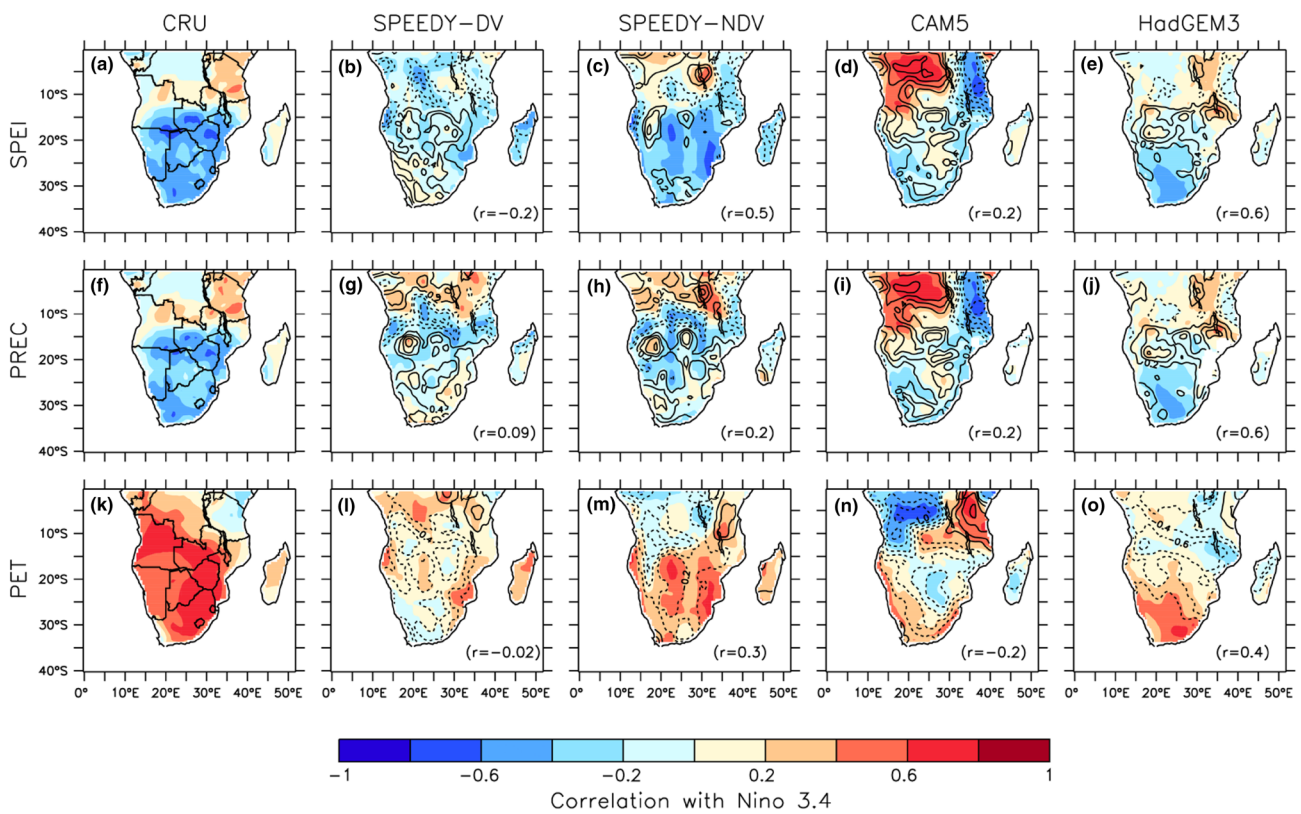


**Fig. 5** The spatial distribution of temporal correlation of the Niño 3.4 Index with 3-month SPEI, precipitation, and PET for the summer season (DJF) during the period 1979–2008, as observed by CRU and simulated by SPEEDY (dynamic and non-dynamic vegetation ver-

sions: SPEEDY\_DV and SPEEDY\_NDV) and other more complex GCMs (HadGEM3 and CAM5). The contours show the correlation bias at intervals of 0.2 and the spatial correlation (r) between the simulation and observation is indicated in brackets

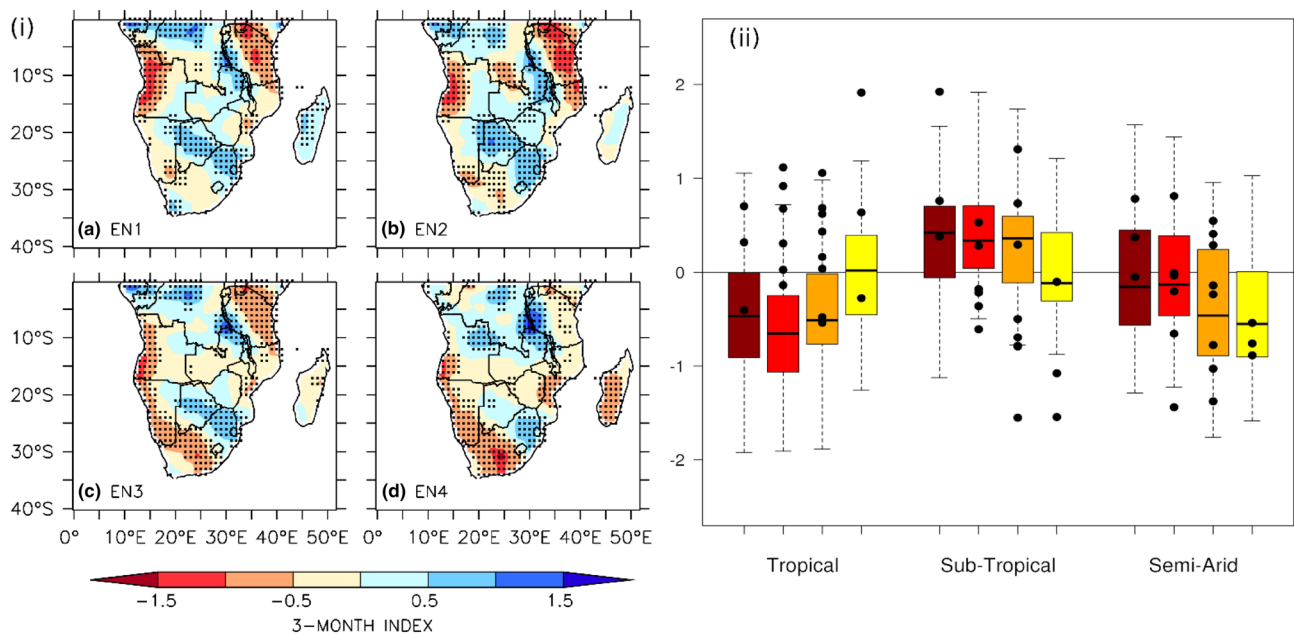


**Fig. 6** **a** Ensemble mean of the DJF 3-month SPEI for the El Niño SST conditions. Stippling indicates values significant at the 99th percentile. **b** Boxplots showing the ensemble spread of the DJF 3-month SPEI for the El Niño patterns in the three areas: tropical, subtropical

and semi-arid. The box represents the interquartile range (first quartile, median and third quartile) and the whiskers represent the extreme minimum and maximum values. The black dots indicate the observed events for each pattern from CRU data

has the best agreement with CRU observation, with most of the observations falling within the ensemble range. Overall, EN2 produces the strongest drought (lowest SPEI) in the tropical area, whereas EN4 shows the strongest drought in the subtropical and semi-arid areas, although the signal in the subtropical area is uncertain.

In order to assess the differences between the ENSO conditions and their associated atmospheric teleconnections, the divergent (velocity potential) and rotational (streamfunction) components of flow, horizontal wind and moisture flux anomalies are investigated.

The El Niño conditions show significant changes in the upper tropospheric divergent flow (velocity potential, Fig. 7). All of the El Niño conditions show a significant upper tropospheric divergence anomaly (negative velocity potential) over the eastern South Pacific Ocean and South America. This negative anomaly extends over the North

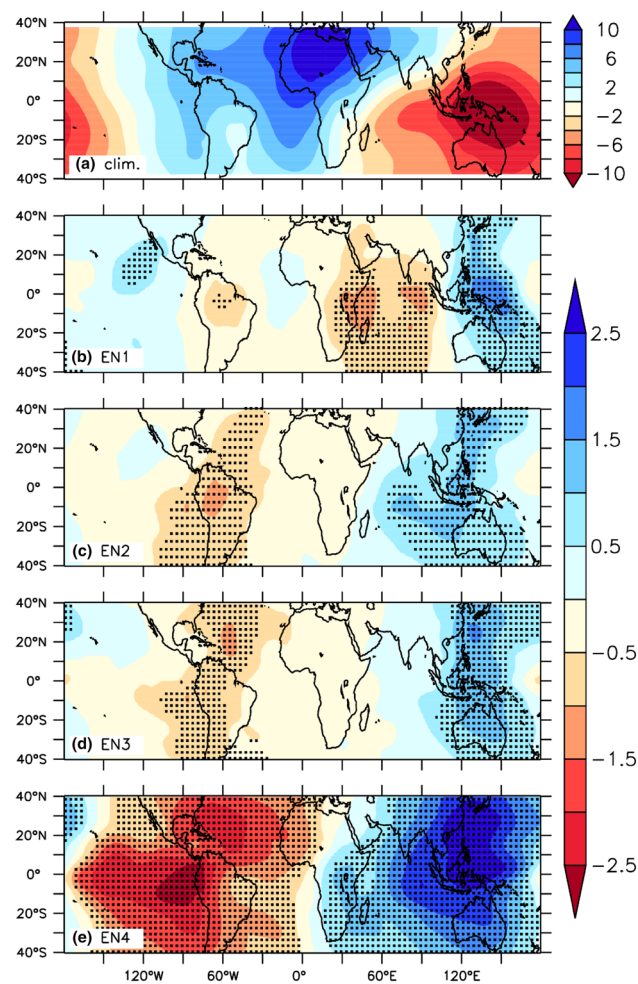


**Fig. 7** 200 hPa velocity potential ( $\times 10^6 \text{ m}^2/\text{s}$ ) for a DJF climatology averaged over the period 1979–2008 and **b–e** composite anomalies for each of the El Niño conditions. Positive values indicate convergent flow and negative values indicate divergent flow. Stippling indicates DJF velocity potential anomalies significant at the 99th percentile

Atlantic Ocean in EN2, EN3 and EN4. The El Niño conditions also show a divergence anomaly over the central Pacific Ocean which coincides with deep convection from the warm SST anomaly, however, only EN4 is significant in this region. In contrast, there is a significant upper tropospheric convergence anomaly (positive velocity potential) over the western Pacific Ocean, including Australia and the Maritime continent, which coincides with cool SST anomaly. This upper tropospheric convergence-divergence anomaly pattern across the Pacific Ocean is a clear indication of a weakening or shift in the Walker Circulation, which is expected during El Niño (Tyson and Preston-Whyte 2000; Reason and Jagadheesha 2005; Ashok et al. 2007; Yuan et al. 2014). EN4 has the most significant velocity potential anomalies, indicating the most significant weakening of the Walker Circulation. EN2 and EN3 have similar velocity potential anomalies, although not as strong as EN4. In EN2, EN3 and EN4, the upper tropospheric convergence anomaly also extends over the Indian Ocean (significant in EN2 and EN4) and is still significant over southern Africa in EN4. This anomalous convergence over the Indian Ocean results in a north-eastward shift of the South Indian Ocean Convergence Zone (Cook 2001) and tropical temperate trough systems (Tyson and Preston-Whyte 2000), contributing to the dry conditions across southern Africa during El Niño. However, the upper tropospheric velocity potential anomalies of EN1 are notably different to the other El Niño conditions. EN1 has a significant divergence anomaly across the Indian Ocean and the eastern coast of Africa. It also shows a convergence anomaly in the eastern Pacific Ocean ( $90^\circ\text{W}$ – $160^\circ\text{W}$ ), which is significant off the coast of North America, characteristic of a central Pacific El Niño (Wilson et al. 2014).

Figure 8 shows the eddy streamfunction (zonal mean removed) for each of the El Niño conditions which emphasizes the large-scale stationary wave response. All of the El Niño conditions show a pair of anticyclonic anomalies in the upper troposphere over the central and eastern Pacific Ocean. This is characteristic of a Gill-Matsuno type response which is expected due to the warm SST anomalies in the tropical Pacific Ocean associated with El Niño (Cook 2001; Wilson et al. 2014). This indicates a significant weakening of the cyclonic flow in the eastern Pacific Ocean and as such a weakening of the Walker Circulation. The strength of the anticyclonic anomaly and weakening of the Walker Circulation is proportional to the intensity of the ENSO SST anomaly associated with each El Niño condition, with EN4 showing the most significant anomaly. There is also a significant pair of cyclonic anomalies in the upper troposphere over the Indian Ocean and Asia, evident in all of the El Niño conditions. However, the size and position of these cyclonic anomalies varies between the conditions. EN1, EN3 and EN4 show the cyclonic anomaly positioned over

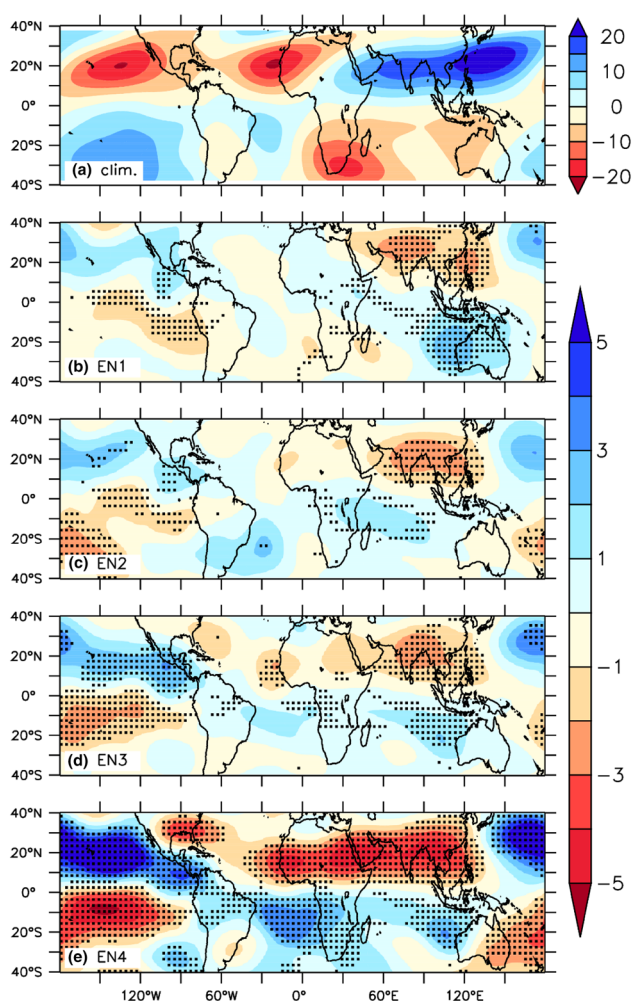


**Fig. 8** 200 hPa eddy stream function ( $\times 10^6 \text{ m}^2/\text{s}$ ) for **a** DJF climatology averaged over the period 1979–2008 and **b–e** composite anomalies for each of the El Niño conditions. Positive values indicate clockwise rotation and negative values indicate anticlockwise rotation. Stippling indicates DJF eddy stream function anomalies significant at the 99th percentile

the eastern Indian Ocean, whilst EN2 shows the anomaly over the western Indian Ocean and tropical region of Africa. EN2, EN3 and EN4 show that the pair of cyclonic anomalies also extend across Africa and the Atlantic Ocean. This results in anomalous cyclonic flow in the upper troposphere over southern Africa, weakening the anticyclonic flow seen over the region during austral summer. In contrast, EN1 significantly strengthens the anticyclonic flow in the upper troposphere over southern Africa.

The El Niño SST conditions are associated with significant changes in the global wind circulation. All of the El Niño conditions show a significant weakening of the Walker circulation. This is indicated by westerly anomalies in the lower troposphere and easterly anomalies in the upper troposphere across the tropical Pacific Ocean basin (Fig. 9). This

response is typical of El Niño and agrees with previous studies (Tyson and Preston-Whyte 2000; Reason and Jagadheesha 2005; Ashok et al. 2007; Yuan et al. 2014). However, the magnitude of this weakening is directly proportional to the strength of the warm SST anomaly in the Pacific Ocean, with EN1 showing the least and EN4 showing the most significant changes. In the upper troposphere, the easterly anomaly in the equatorial region lends itself to anticyclonic circulation across the Pacific Ocean in both hemispheres. This results in the significant strengthening of the subtropical jet stream as seen in EN3 and EN4. Over the tropical Indian Ocean, there is an easterly anomaly in the lower troposphere (most significant in EN1 and EN4), which is a result of diverging air over the Maritime Continent from the descending limb of the Walker Circulation. This anomaly is strengthened in EN4 by the presence of the positive IOD. Over Africa, EN1 is associated with a significant upper tropospheric easterly anomaly over the equatorial region, which in turn strengthens the Tropical Easterly Jet (TEJ). In the lower troposphere, there are no significant changes to the circulation over southern Africa, however, there is a weak cyclonic anomaly over the Mozambique Channel. EN2 is associated with a significant easterly anomaly over the equatorial region at 850 hPa and a weak anticyclonic anomaly over the west coast of southern Africa, which is also seen at 200 hPa. There is also a notable anticyclonic anomaly over the south-western Indian Ocean, which extends over the eastern part of the continent. In the upper troposphere, EN3 and EN4 are associated with westerly anomalies across Africa and the Atlantic and Indian Oceans, although only significant in EN4. There are no clear circulation patterns associated with EN3 in the lower atmosphere, however, EN4 shows a weak anticyclonic anomaly over the Mozambique Channel.

There are variations in the moisture flux divergence over southern Africa associated with each El Niño SST condition. Figure 10 shows that the vertically integrated moisture flux for the El Niño conditions is characterized by a lower tropospheric anticyclonic flow anomaly over southern Africa. This results in the typical dry conditions associated with El Niño, previously reported by studies (Tyson and Preston-Whyte 2000; Ashok et al. 2007; Davis 2011; Hoell et al. 2015; Yuan et al. 2014). However, the location and intensity of the anticyclonic moisture flux varies between the El Niño conditions, resulting in the variations seen in the drought patterns (Fig. 6). EN1 and EN3 show the anticyclonic moisture flow anomaly over the central region, whereas EN2 shows stronger anticyclonic circulation in a more northerly position and EN4 shows an elongated circulation in a more south easterly position. These anticyclonic moisture flow anomalies are associated with divergence (Fig. 10), resulting in dry conditions in their respective areas. EN1 shows cyclonic moisture flow anomaly over the Mozambique Channel,

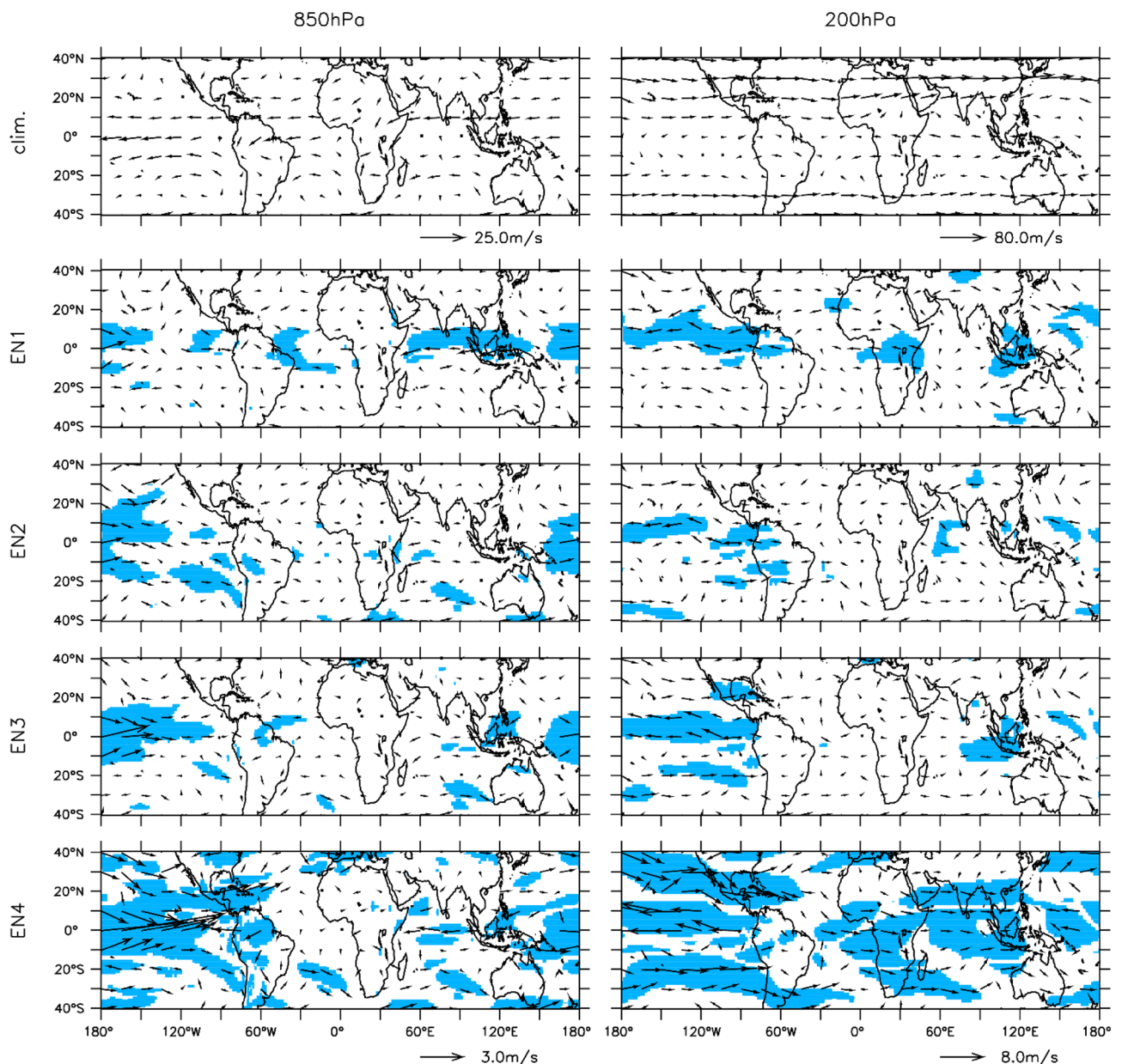


**Fig. 9** 850 hPa and 200 hPa wind vectors (m/s) for DJF climatology averaged over the period 1979–2008 and composite wind vector anomalies for each of the El Niño conditions. Shading indicates DJF wind speed anomalies significant at the 99th percentile

whilst EN2 shows anticyclonic moisture flow anomaly in that region. The two anticyclonic flow anomalies in EN2 cause significant divergence over Tanzania, resulting in severe drought conditions (seen in Fig. 6). They also cause an increase in convergence in the central region across Zambia, Botswana and Zimbabwe, resulting in widespread wet conditions seen in this region during EN2. There is a progressive increase in the westerly moisture flow anomaly in the southern region throughout the El Niño conditions, with EN1 showing the least anomaly and EN4 showing

the strongest westerly flow anomaly. This is associated with a progressive increase in the extent of divergence seen across the southern part of the region, as well as a gradual increase in the intensity and extent of drought in the region (seen in Fig. 6). Unlike the other El Niño conditions, EN4 shows onshore moisture flux from the tropical Atlantic Ocean. This converges with the onshore flux from the Mozambique channel, resulting in notable convergence and wet conditions over Angola and the Congo basin.

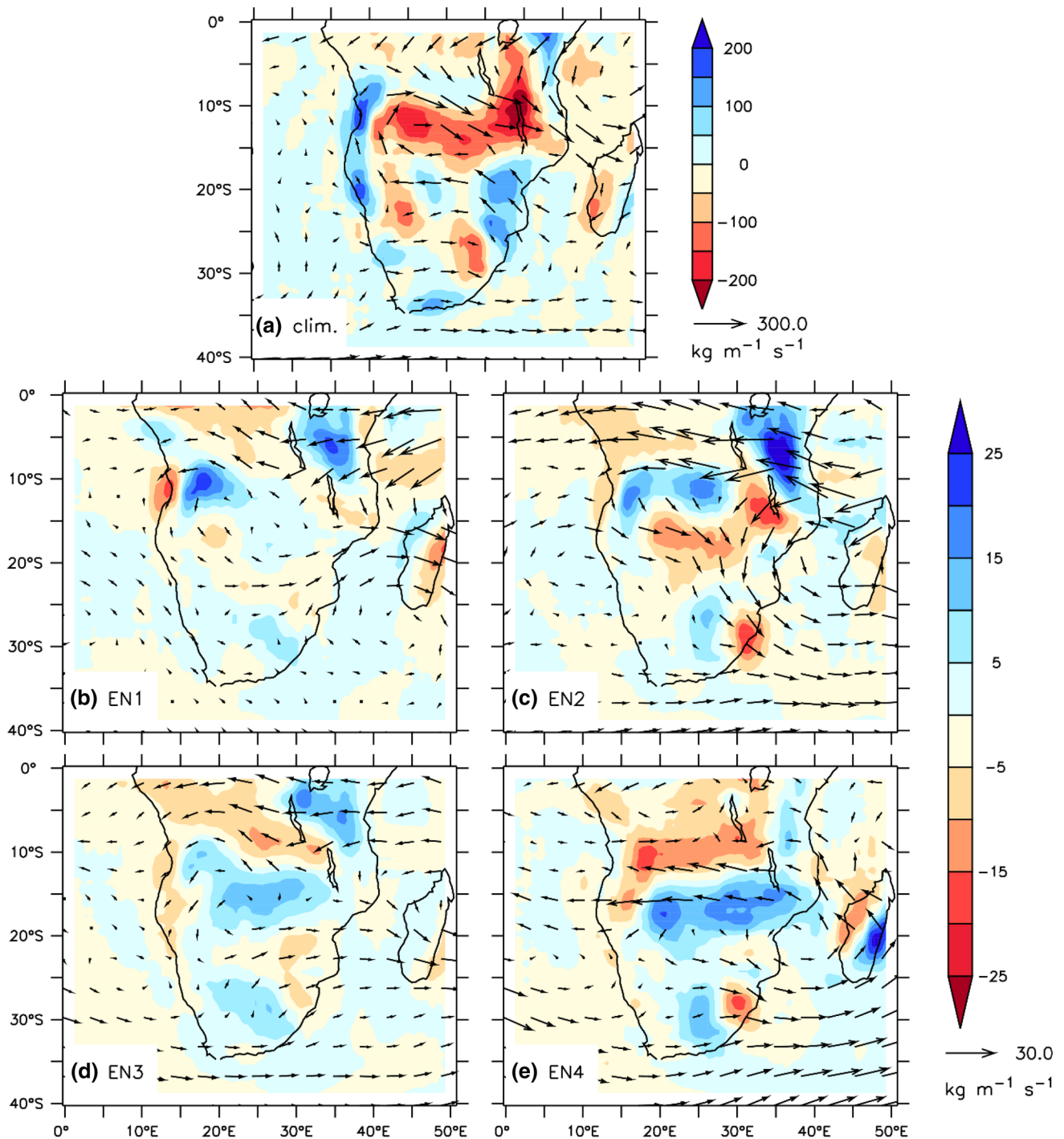


**Fig. 10** Vertically integrated moisture flux divergence ( $\times 10^{-6} \text{ kg m}^{-2} \text{ s}^{-1}$ ) and vertically integrated moisture flux vectors ( $\text{kg m}^{-1} \text{ s}^{-1}$ ) between 850 hPa to 500 hPa for **a** DJF climatology aver-

aged over the period 1979–2008 and **b–e** composite anomalies for each of the El Niño conditions. This figure was not screened for significance

### 3.2.2 Drought and atmospheric dynamics associated with La Niña conditions

The La Niña results show a distinct dipole pattern in SPEI drought across southern Africa, although there is variation

in the spatial pattern and intensity between the La Niña conditions (Fig. 11). Across all the La Niña conditions there is a significant positive anomaly in the central/southern part of the subcontinent with a negative anomaly stretching across the tropical region ( $\sim 5\text{--}10^\circ\text{S}$ ). The positive

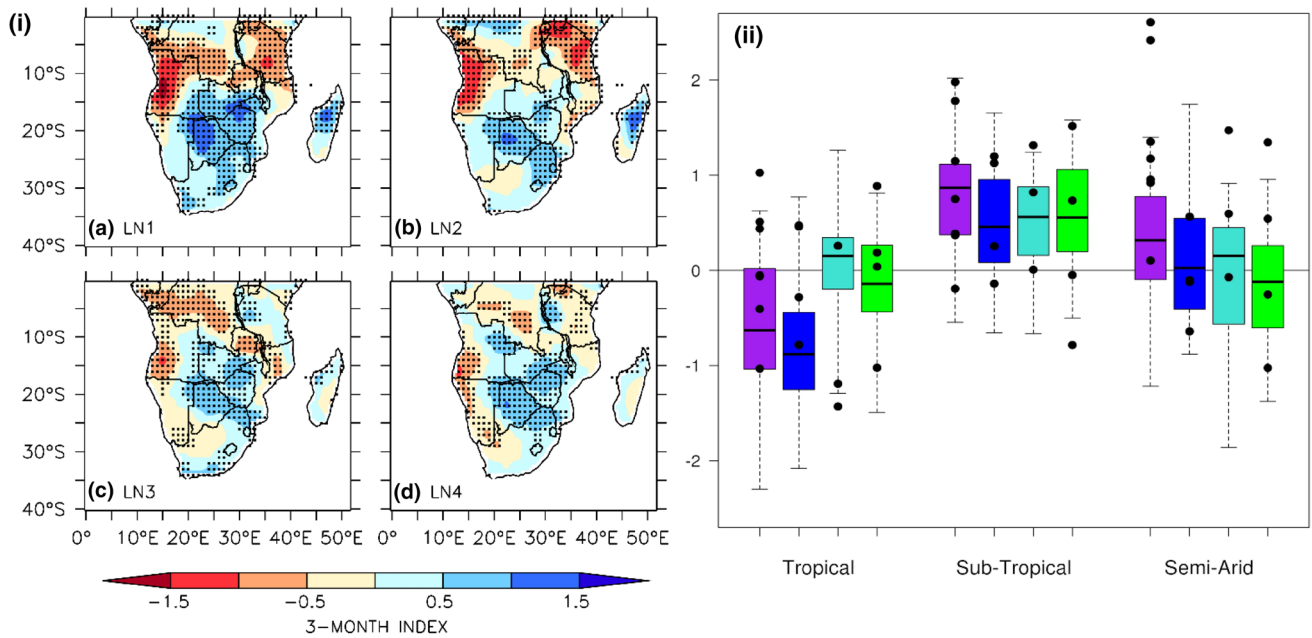


**Fig. 11** Same as Fig. 6, but for the La Niña conditions

anomaly ( $\text{SPEI} > 0.5$ ) is focused over Botswana, Zimbabwe and north-eastern South Africa with LN1 showing the strongest ( $\text{SPEI} > 1$ ) and most widespread signal including the whole of South Africa (Fig. 11a). The other La Niña conditions all show a similar positive anomaly, with LN3 (Fig. 11c) also showing significant positive SPEI along the southern coast. LN1 shows the strongest negative anomaly in the tropical region with SPEI drought greater than  $-1.5$  in parts of Angola. LN2 (Fig. 11b) also shows a significant negative anomaly in the tropical region, although not as widespread in the central areas. On the other hand, LN3 and LN4 (Fig. 11c, d) show a weaker ( $\text{SPEI} < -0.5$ ), but still significant negative anomaly in the tropical region. However, the negative anomaly spreads over the Congo basin and down the western coast into South Africa during LN3 and LN4. Overall, LN1 shows the strongest dipole pattern whilst LN4 shows the weakest signal. The general dipole pattern seen in Fig. 11 corresponds with the literature (Tyson and Preston-Whyte 2000; Meque and Abiodun 2015; Hoell et al. 2015), which typically associates La Niña phases with wet conditions across most of the sub-region and dry conditions in the tropical region.

There is variation in the uncertainty of the drought signal across the different areas as shown in the ensemble spread of the La Niña conditions (Fig. 11). In the tropical area, LN1 and LN2 show a high probability of drought with at least 75% of the ensemble giving a negative SPEI value. LN2 indicates the most severe drought where approximately 50% of the ensemble has an SPEI value less than  $-1$ . This agrees with studies (Nicholson and Selato 2000; Reason and

Jagadheesha 2005) which show that dry conditions typically develop over the tropical area during La Niña phases. However, this does not fully agree with the observed CRU events which generally show higher SPEI values, mostly within the upper two quartiles of the ensemble spread. On the other hand, LN3 and LN4 remain uncertain in their signal, as the ensemble SPEI values range between 1 and  $-1$ . There is a strong probability of wet conditions in the subtropical region during the La Niña phase, with more than 75% of the ensembles showing positive SPEI anomalies across all La Niña conditions. Although it is hard to distinguish this signal from the precipitation bias which SPEEDY simulates. However, this might not be the case as the ensemble spread has very good agreement with the observed CRU events. The SPEI results in the semi-arid area have the biggest ensemble spread and are uncertain. LN1 shows the most definite signal of positive SPEI, although it is less than 75% of the ensemble. The semi-arid area also shows the least agreement with CRU observation, generally producing SPEI values lower than observed.

The La Niña conditions show significant changes in the upper tropospheric divergent flow (velocity potential, Fig. 12). All of the La Niña conditions show a significant upper tropospheric convergence anomaly (positive velocity potential) over the central and eastern Pacific Ocean, with LN2 showing the weakest anomaly and LN3 showing the strongest anomaly. This anomaly strengthens upper tropospheric convergence as a result of strong subsidence associated with the underlying cold SST anomalies. There is also a significant upper tropospheric divergence anomaly

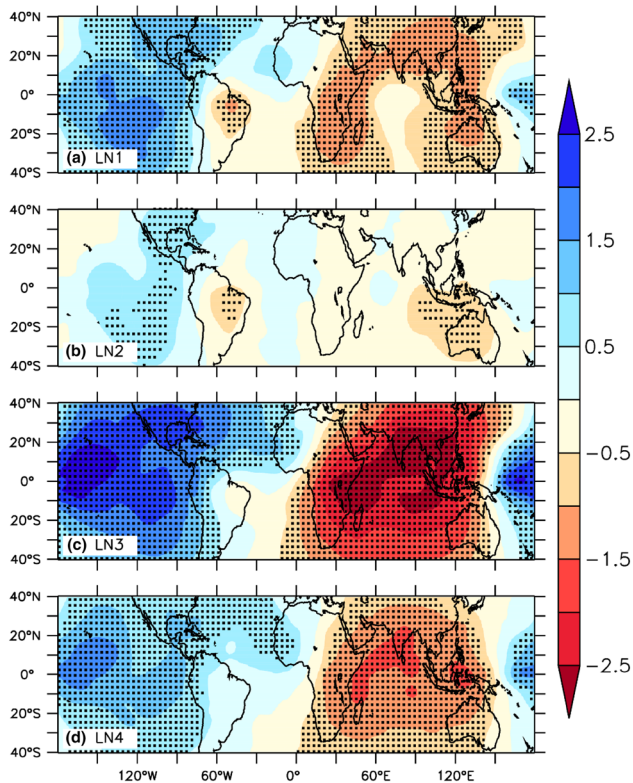


**Fig. 12** Same as Fig. 7, but for the La Niña conditions

over the western Pacific Ocean, Australia and the Maritime continent, which corresponds with warm SST anomalies in the region. This upper tropospheric divergence-convergence anomaly across the Pacific Ocean strengthens the austral summer velocity potential pattern and further indicates a strengthening of the Walker Circulation. LN3 shows the most significant strengthening of the Walker Circulation. The convergence anomaly over the eastern Pacific extends across North America and the North Atlantic Ocean and is strongest in LN3. LN3 and LN4 also show the convergence anomaly over South America which is significant along the western coast. In contrast, LN1 and LN2 show an upper tropospheric divergence anomaly centred over Brazil. There is a significant divergence anomaly extending across the Indian Ocean, Asia and Africa during LN3 and LN4, which is strengthened by the warm SST anomalies in the region. LN1 also shows significant divergence anomalies over the Indian Ocean, but not in the central region due to cold SST anomalies. LN2 also has cold SST anomalies across the Indian Ocean resulting in minimal changes to velocity potential, except for a small area of significant divergence in the eastern region. Generally, southern Africa experiences anomalous divergent flow in the upper troposphere, which is significant in LN1, LN3 and LN4, with LN3 showing the strongest anomaly. This strengthens the South Indian Ocean Convergence

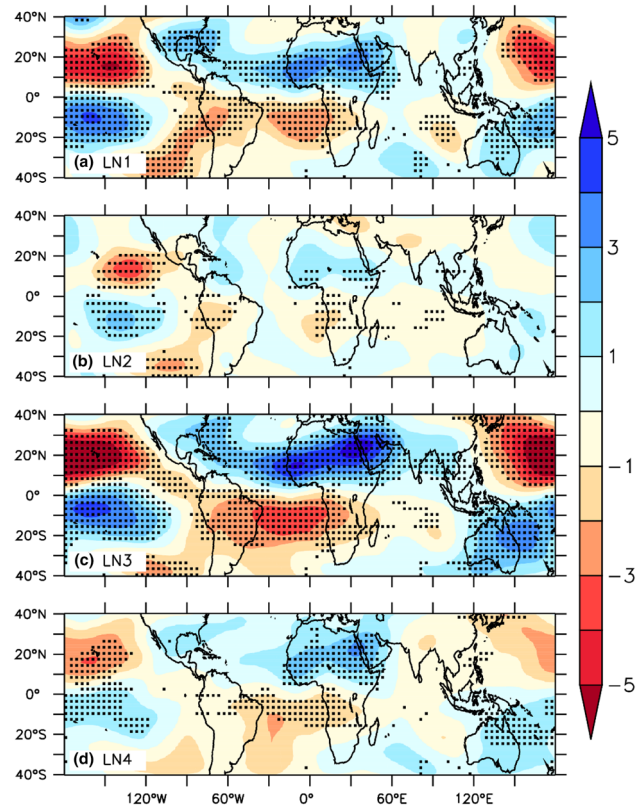


**Fig. 13** Same as Fig. 8, but for the La Niña conditions

Zone and encourages the formation of tropical temperate troughs during La Niña (Tyson and Preston-Whyte 2000).

There are significant anomalies in the upper tropospheric rotational flow (eddy streamfunction) associated with the La Niña conditions (Fig. 13). There is a significant strengthening of the cyclonic flow in the upper troposphere over the central and eastern Pacific Ocean, shown by a pair of cyclonic anomalies, which are associated with the intensity of the cold SST anomaly in the region. LN3 has the strongest anomaly and the cyclonic flow extends as far as the western Pacific Ocean in LN1 and LN3. On the other hand, LN2 has the weakest anomaly and is limited to the eastern Pacific Ocean. There is a pair of significant upper tropospheric anticyclonic anomalies extending across Africa, the Atlantic Ocean and North and South America. LN3 shows the strongest anticyclonic anomalies, whilst LN2 shows the weakest anomalies which are primarily focused over Africa. Generally, the Indian Ocean also experiences anticyclonic anomalies, however they are not as strong as those over the Atlantic Ocean. LN1 also shows a significant upper tropospheric cyclonic anomaly over the South Indian Ocean, which is also seen in the other La Niña conditions, although not significant. Southern Africa is generally characterized by a significant upper tropospheric anticyclonic anomaly over the tropical region, which is most notable in LN3. However,

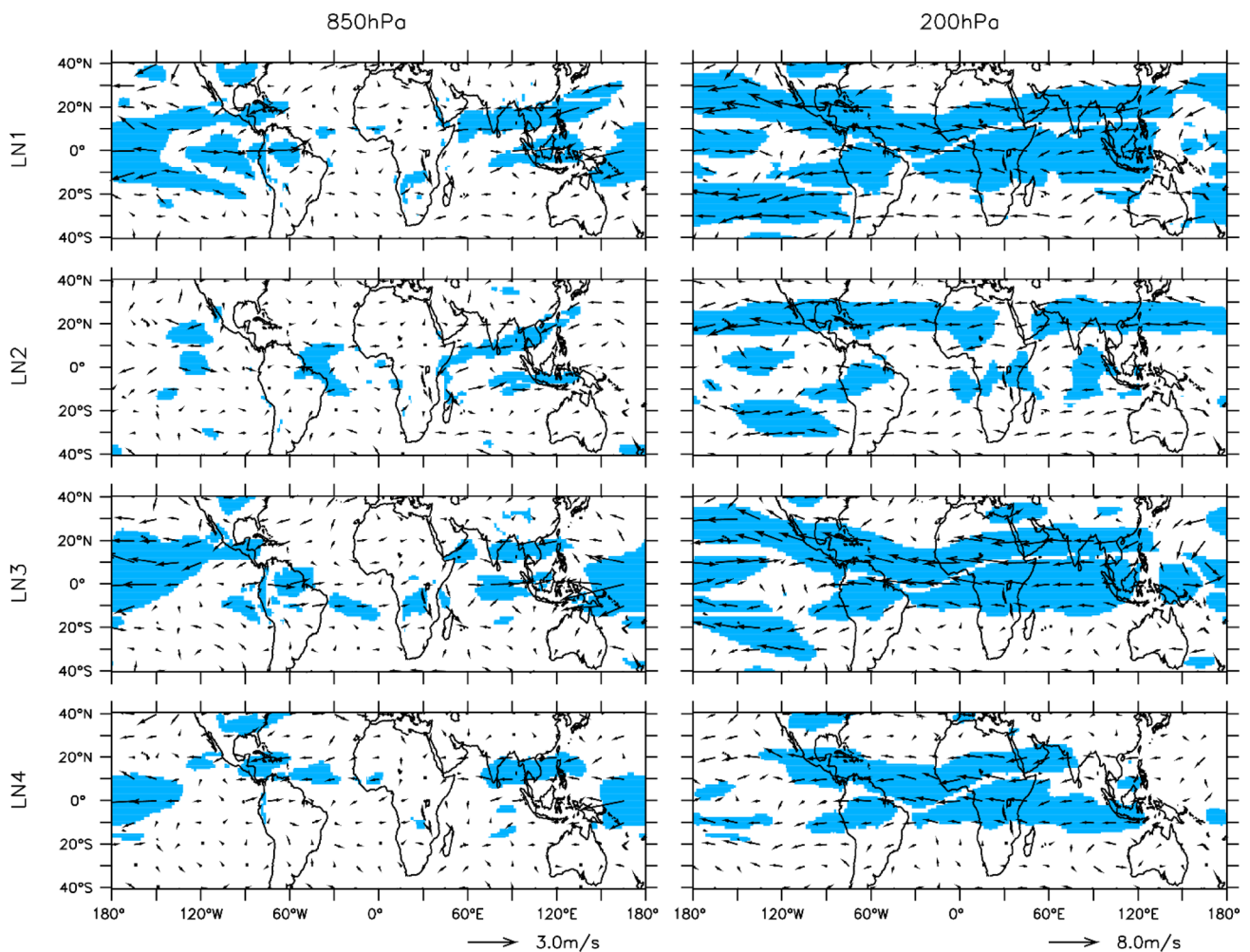


**Fig. 14** Same as Fig. 9, but for the La Niña conditions

the southern tip of Africa shows an upper tropospheric cyclonic anomaly in LN1, LN2 and LN4, although not significant. This indicates a northward shift of the anticyclonic flow typically seen over southern Africa in austral summer (Fig. 8).

The La Niña SST conditions are also associated with significant changes in the global wind circulation. Most notably is the strengthening of the Walker circulation seen in all of the La Niña conditions. This is generally shown by easterly anomalies in the lower troposphere and westerly anomalies in the upper troposphere across the tropical Pacific Ocean basin (Fig. 14). This is a typical atmospheric response to La Niña as shown by previous studies (Tyson and Preston-Whyte 2000; Reason and Jagadheesha 2005; Ashok et al. 2007; Yuan et al. 2014), however, the intensity of this anomaly varies between the conditions. LN1 and LN3 show the most significant strengthening of the Walker Circulation, whilst LN2 shows the least change in the lower troposphere and LN4 shows the least change in the upper troposphere

over the Pacific Ocean. LN1, LN2 and LN3 also show significant westerly anomalies over the eastern Pacific Ocean and/or South America at 850 hPa as a result of diverging air caused by the descending limb of the Walker Circulation over the central Pacific Ocean. In contrast to El Niño, the La Niña conditions have a more significant influence on the upper tropospheric wind circulation, particularly over Africa and the Indian and Atlantic Oceans. This robust modification of the Walker Circulation explains the stronger SPEI response over southern Africa during the La Niña SST conditions, compared to El Niño. All of the La Niña conditions show significant easterly anomalies globally in the upper troposphere, which result in a weakening of the subtropical westerly jet stream and strengthening of the TEJ. In the lower troposphere, there are cyclonic circulation anomalies over the Indian Ocean in both hemispheres. This results in a significant westerly anomaly along the equator and easterly anomalies in the subtropical regions, although more significant in the northern part of the ocean basin. This circulation

anomaly is strongest in LN3, due to the presence of the negative IOD, and weakest in LN4. The tropical Atlantic Ocean shows lower tropospheric westerly anomalies in LN3 and LN4, although only significant in LN3, and easterly anomalies in LN2. Southern Africa is generally characterized by cyclonic circulation in the lower troposphere for all of the La Niña conditions, resulting in significant westerly flow over the tropical part of the region. In the upper troposphere, LN1 and LN2 are dominated by an easterly anomaly across southern Africa, whereas LN3 and LN4 show minimal circulation anomalies over the southern part of the region.

Each La Niña condition shows variations in the vertically integrated moisture flux divergence over southern Africa, resulting in notable differences in the drought patterns. The La Niña conditions are generally characterized by lower tropospheric cyclonic moisture flow anomaly over the central part of the region (Fig. 15). This results in significant convergence and increased precipitation in the region, including Zambia, Zimbabwe and Botswana. This agrees with previous studies, which show that La Niña is generally associated with pluvial conditions in these regions (Tyson

and Preston-Whyte 2000; Ashok et al. 2007; Davis 2011; Hoell et al. 2015; Yuan et al. 2014). The position of the convergence associated with the cyclonic flow anomaly is indicative of a southward shift of the ITCZ during La Niña. There are no notable changes in the size or position of the cyclonic flow anomaly between the La Niña conditions. However, there is variation in its intensity with LN1 showing the strongest and LN2 showing the weakest anomaly. This cyclonic flow anomaly is collocated with significant divergence to the north which varies with the position and intensity of the onshore moisture flux from the tropical Atlantic Ocean. LN3 and LN4 show significant onshore flux from the Atlantic Ocean throughout the tropical region ( $0^{\circ}$ – $16^{\circ}$ S), with LN3 showing the strongest flux. This results in a divergence anomaly and drought conditions over the central and western equatorial region (Congo basin) and increased convergence over the eastern equatorial region (Tanzania). On the other hand, LN1 and LN2 show a weaker onshore moisture flow from the Atlantic Ocean which is not as prevalent in the equatorial region. This results in divergent anticyclonic moisture flow and significant drought primarily over

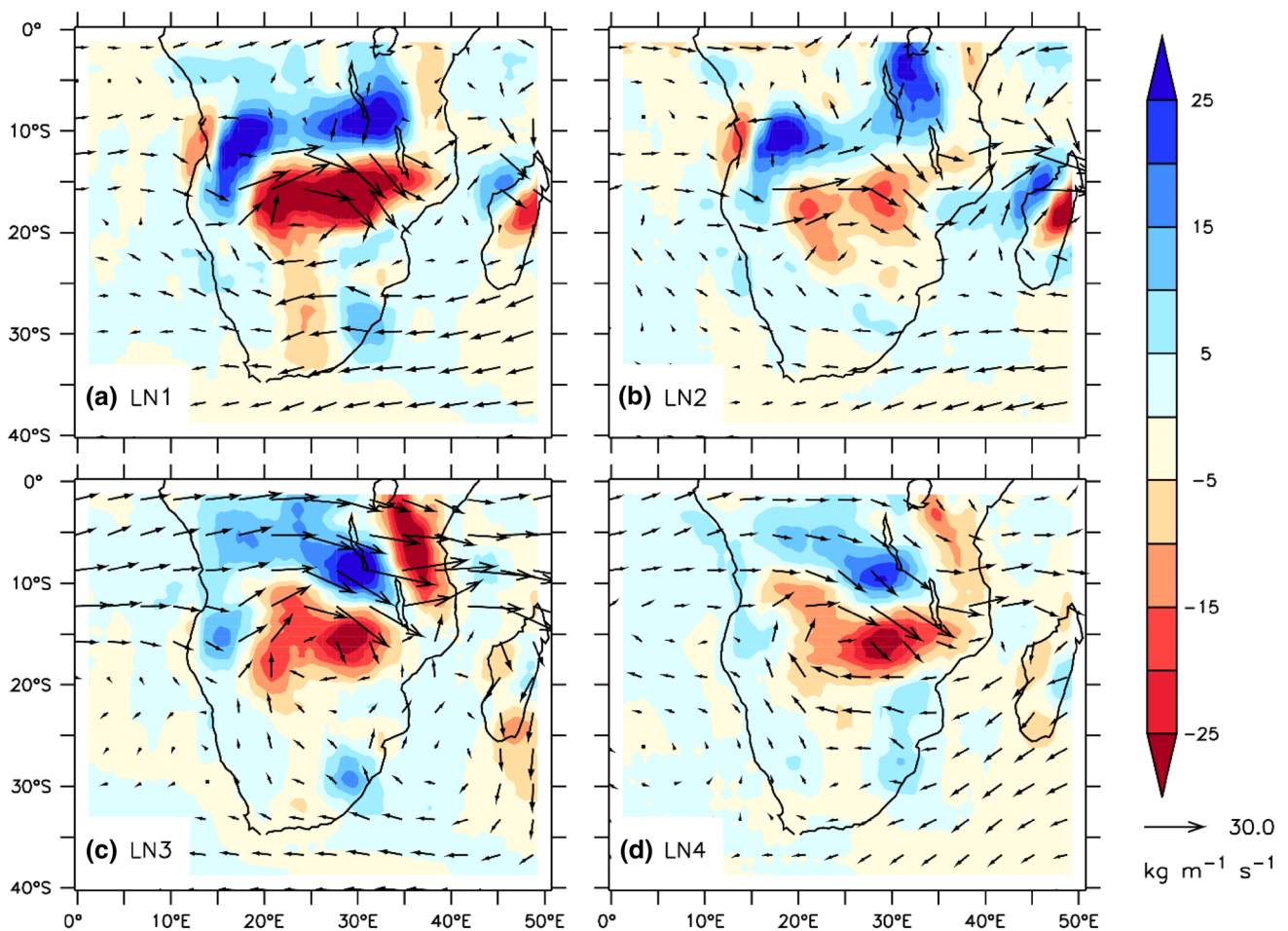


Fig. 15 Same as Fig. 10, but for the La Niña conditions

Angola, as well as divergence across the southern tropical region and Tanzania. This agrees with Nicholson and Kim (1997) who emphasize the influence of the Atlantic Ocean on southern Africa climate during the La Niña conditions, whilst the El Niño conditions are more strongly influenced by the Indian Ocean. All of the La Niña conditions show divergence along the western coast; however, only LN3 and LN4 result in significant drought in this region (seen in Fig. 11). This is a result of the low moisture flux from the southern Indian Ocean, compared to the strong onshore flux during LN1 and LN2 which inhibits significant drought. LN3 also shows cyclonic moisture flow anomaly over the Mozambique Channel, resulting in significant wet conditions along the southern coast (Fig. 11).

#### 4 Discussion and conclusion

In an effort to better understand the nonlinear impacts of ENSO on southern Africa climate, this study has investigated the relationship between southern Africa drought and eight ENSO SST patterns. We analysed multi-forcing ensemble simulations from SPEEDY, an AGCM of intermediate complexity from the ICTP. SPEEDY simulations were forced with SST from each of the eight ENSO SST patterns previously identified by Johnson (2013) and Hoell et al. (2015). The capability of SPEEDY in reproducing southern Africa summer climate was evaluated by comparing the historical simulations (1979–2008) with CRU observation. The influence of each ENSO pattern on southern Africa drought was then explored in terms of the simulated drought index (SPEI) and associated atmospheric dynamics.

Results of the study can be summarised as follows:

- SPEEDY generally captures characteristics of summer climate (DJF) over southern Africa well, albeit with warm and wet biases across the region. However, in most cases, these results are comparable with those from more complex atmospheric models.
- The SPEEDY simulation without the dynamic vegetation scheme tends to perform better than SPEEDY with dynamic vegetation in most instances, especially in the tropical and subtropical areas.
- The El Niño (La Niña) SST conditions typically result in negative (positive) SPEI and dry (wet) conditions over parts of southern Africa. However, the robustness of the SPEI signal varies across the different areas.
- The drought patterns are primarily driven by a weakening (strengthening) of the Walker circulation associated with the strength of the El Niño (La Niña) SST anomaly in the Pacific Ocean. However, variations in the Indian Ocean and Atlantic Ocean have a strong moderating

effect which alters the circulation, thereby influencing the spatial pattern and intensity of drought over the region.

- The El Niño SST conditions feature different characteristics of anticyclonic moisture flux over southern Africa which induce drought in different regions. EN1 and EN2 produce drought primarily in the tropical region whilst EN3 and EN4 show drought in the southwestern region.
- The La Niña SST conditions show a distinct dipole pattern in the drought, with significant wet conditions over the subtropical region driven by cyclonic moisture flux anomaly. Differences in the SPEI drought occur due to variations in the onshore flux from the southern Indian Ocean and tropical Atlantic Ocean, with LN1 and LN2 producing drought in the northern part, whilst LN3 and LN4 show drought along the western coast.

The results of the study further affirm the idea that ENSO is a main source of southern Africa climate predictability (Nicholson and Entekhabi 1987; Lindsay 1988; Nicholson and Kim 1997; Reason et al. 2000; Cook 2001; Reason and Jagadheesha 2005). The study shows that while a simple GCM (such as SPEEDY) can capture the general influence of ENSO on drought in southern Africa, both simple and complex climate models struggle to provide the detailed influence of ENSO on the inter-annual variability of austral summer droughts. This is also a challenge to some RCMs (Meque and Abiodun 2015). The study performs climate simulations to confirm the observational evidence of Hoell et al. (2015) that southern African droughts respond differently to the different flavours of El Niño (or La Niña) SST patterns, reinforcing the importance of SST anomalies within the Indian Ocean and the Atlantic Ocean in modulating rainfall over southern Africa. However, the study has expanded on the work of Hoell et al. (2015) by studying the influence of the ENSO SST patterns on SPEI (instead of rainfall), thereby including the impact of evaporative demand on drought severity. This study also strengthens the observational results of Hoell et al. (2015) by using an ensemble modelling framework to assess the robustness of the ENSO influence on southern Africa drought.

Nevertheless, the results of this study can be improved in many ways. Most notably, the warm and wet bias SPEEDY produces over parts of southern Africa needs to be improved. This will reduce the uncertainty and improve the reliability of the results, particularly in areas such as the subtropical region where dry conditions are expected during El Niño phases, but SPEEDY simulates wet conditions. As seen in the model evaluation, climate models with higher resolution and complexity do produce more realistic simulations of the southern Africa climate, particularly precipitation, although they do also show some biases. Therefore, in order to improve these results, future research should consider using a more complex climate model with higher resolution,

provided that such a model is accessible. Nevertheless, the present study shows that accounting for differences in ENSO SST patterns may improve drought predictions in southern Africa.

**Acknowledgements** The project was supported by grants from the National Research Foundation (NRF, South Africa) and the Alliance for Collaboration on Climate and Earth Systems Science (ACCESS, South Africa). We thank the Abdus Salam International Centre for Theoretical Physics for making SPEEDY available and for providing technical support. We would also like to thank the two anonymous reviewers for their constructive feedback.

## References

- Abiodun BJ, Makhanya N, Petja B, Abatan AA, Oguntunde PG (2019) Future projection of droughts over major river basins in Southern Africa at specific global warming levels. *Theor Appl Climatol* 137(3–4):1785–1799
- Angéilil O, Stone D, Wehner M, Paciorek CJ, Krishnan H, Collins W (2017) An independent assessment of anthropogenic attribution statements for recent extreme temperature and rainfall events. *J Clim* 30(1):5–16
- Ash KD, Matyas CJ (2012) The influences of ENSO and the subtropical Indian Ocean Dipole on tropical cyclone trajectories in the southwestern Indian Ocean. *Int J Climatol* 32(1):41–56
- Ashok K, Behera SK, Rao SA, Weng HY, Yamagata T (2007) El Niño Modoki and its possible teleconnection. *J Geophys Res Oceans* 112(C11):C11007
- Bahaga TK, Mengistu Tsidu G, Kucharski F, Diro GT (2015) Potential predictability of the sea-surface temperature forced equatorial East African short rains interannual variability in the 20th century. *Q J R Meteorol Soc* 141(686):16–26
- Beguéría S, Vicente-Serrano SM (2013) SPEI: calculation of the standardised precipitation- evapotranspiration index. R package version, 1
- Beguéría S, Vicente-Serrano SM, Reig F, Latorre B (2014) Standardized precipitation evapotranspiration index (SPEI) revisited: parameter fitting, evapotranspiration models, tools, datasets and drought monitoring. *Int J Climatol* 34(10):3001–3023
- Behera SK, Yamagata T (2001) Subtropical SST dipole events in the southern Indian Ocean. *Geophys Res Lett* 28(2):327–330
- Bourke W (1974) A multi-level spectral model. I. Formulation and hemispheric integrations. *Mon Weather Rev* 102(10):687–701
- Bracco A, Kucharski F, Kallummal R, Molteni F (2004) Internal variability, external forcing and climate trends in multi-decadal AGCM ensembles. *Clim Dyn* 23(6):659–678
- Bracco A, Kucharski F, Molteni F, Hazeleger W, Severijns C (2007) A recipe for simulating the interannual variability of the Asian summer monsoon and its relation with ENSO. *Clim Dyn* 28(5):441–460
- Bulić IH, Kucharski F (2012) Delayed ENSO impact on spring precipitation over North/Atlantic European region. *Clim Dyn* 38(11–12):2593–2612
- Calow RC, MacDonald AM, Nicol AL, Robins NS (2010) Ground water security and drought in Africa: linking availability, access, and demand. *Groundwater* 48(2):246–256
- Chretien JP, Anyamba A, Small J, Britch S, Sanchez JL, Halbach AC, Tucker C, Linthicum KJ (2015) Global climate anomalies and potential infectious disease risks: 2014–2015. *PLoS Curr* 7:e2503
- Christidis N, Stott PA, Scaife AA, Arribas A, Jones GS, Copsey D, Knight JR, Tennant WJ (2013) A new HadGEM3-A-based system for attribution of weather- and climate-related extreme events. *J Clim* 26(9):2756–2783
- Ciavarella A, Christidis N, Andrews M, Groenendijk M, Rostron J, Elkington M, Burke C, Lott FC, Stott PA (2018) Upgrade of the HadGEM3-A based attribution system to high resolution and a new validation framework for probabilistic event attribution. *Weather Clim Extrem* 20:9–32
- Cook KH (2000) The South Indian convergence zone and interannual rainfall variability over southern Africa. *J Clim* 13(21):3789–3804
- Cook KH (2001) A Southern Hemisphere wave response to ENSO with implications for southern Africa precipitation. *J Atmos Sci* 58(15):2146–2162
- Davis CL (2011) Climate risk and vulnerability: a handbook for Southern Africa. Council for Scientific and Industrial Research, Pretoria, South Africa
- Davis-Reddy CL, Vincent K (2017) Climate risk and vulnerability: a handbook for Southern Africa, 2nd edn. CSIR, Pretoria
- Dieppois B, Rouault M, New M (2015) The impact of ENSO on Southern African rainfall in CMIP5 ocean atmosphere coupled climate models. *Clim Dyn* 45(9–10):2425–2442
- Dogar MM, Kucharski F, Azharuddin S (2017) Study of the global and regional climatic impacts of ENSO magnitude using SPEEDY AGCM. *J Earth Syst Sci* 126(2):30
- Fauchereau N, Pohl B, Reason CJC, Rouault M, Richard Y (2009) Recurrent daily OLR patterns in the Southern Africa/Southwest Indian Ocean region, implications for South African rainfall and teleconnections. *Clim Dyn* 32(4):575–591
- Feudale L, Kucharski F (2013) A common mode of variability of African and Indian monsoon rainfall at decadal timescale. *Clim Dyn* 41(2):243–254
- Goddard L, Graham NE (1999) Importance of the Indian Ocean for simulating rainfall anomalies over eastern and southern Africa. *J Geophys Res Atmos* 104(D16):19099–19116
- Hargreaves GH, Allen RG (2003) History and evaluation of Hargreaves evapotranspiration equation. *J Irrig Drain Eng* 129(1):53–63
- Hayes MJ, Svoboda MD, Wardlow BD, Anderson MC, Kogan F (2012) Drought monitoring: historical and current perspectives. In: Remote sensing of drought: innovative monitoring approaches. Drought Mitigation Center Faculty Publications, CRC Press/Taylor & Francis
- Held IM, Suarez MJ (1994) A proposal for the intercomparison of the dynamical cores of atmospheric general circulation models. *Bull Am Meteorol Soc* 75(10):1825–1830
- Hoell A, Funk C, Magadzire T, Zinke J, Husak G (2015) El Niño–Southern Oscillation diversity and Southern Africa teleconnections during Austral Summer. *Clim Dyn*. <https://doi.org/10.1007/s00382-014-2414-z>
- Hoell A, Funk C, Zinke J, Harrison L (2017) Modulation of the southern Africa precipitation response to the El Niño Southern Oscillation by the subtropical Indian Ocean dipole. *Clim Dyn* 48(7–8):2529–2540
- Johnson NC (2013) How many ENSO flavors can we distinguish? *J Clim* 26(13):4816–4827
- Kao HY, Yu JY (2009) Contrasting eastern-Pacific and central-Pacific types of ENSO. *J Clim* 22(3):615–632
- Kucharski F, Molteni F, Bracco A (2006) Decadal interactions between the western tropical Pacific and the North Atlantic Oscillation. *Clim Dyn* 26(1):79–91
- Kucharski F, Bracco A, Yoo JH, Tompkins AM, Feudale L, Ruti P, Dell’Aquila A (2009) A Gill–Matsuno-type mechanism explains the tropical Atlantic influence on African and Indian monsoon rainfall. *Q J R Meteorol Soc* 135(640):569–579
- Kucharski F, Bracco A, Barimalala R, Yoo JH (2011) Contribution of the east–west thermal heating contrast to the South

- Asian Monsoon and consequences for its variability. *Clim Dyn* 37(3–4):721–735
- Kucharski F, Molteni F, King MP, Farneti R, Kang IS, Feudale L (2013a) On the need of intermediate complexity general circulation models: a “SPEEDY” example. *Bull Am Meteorol Soc* 94(1):25–30
- Kucharski F, Zeng N, Kalnay E (2013b) A further assessment of vegetation feedback on decadal Sahel rainfall variability. *Clim Dyn* 40(5–6):1453–1466
- Larkin NK, Harrison DE (2005) Global seasonal temperature and precipitation anomalies during El Niño autumn and winter. *Geophys Res Lett* 32(16):L16705
- Li Y, Kalnay E, Motesharrei S, Rivas J, Kucharski F, Kirk-Davidoff D, Bach E, Zeng N (2018) Climate model shows large-scale wind and solar farms in the Sahara increase rain and vegetation. *Science* 361(6406):1019–1022
- Lindesay JA (1988) South African rainfall, the Southern Oscillation and a Southern Hemisphere semi-annual cycle. *J Climatol* 8(1):17–30
- Manatsa D, Mushore T, Lenouo A (2017) Improved predictability of droughts over southern Africa using the standardized precipitation evapotranspiration index and ENSO. *Theor Appl Climatol* 127(1–2):259–274
- Mason SJ, Joubert AM (1997) Simulated changes in extreme rainfall over southern Africa. *Int J Climatol* 17(3):291–301
- Meque A, Abiodun BJ (2015) Simulating the link between ENSO and summer drought in Southern Africa using regional climate models. *Clim Dyn* 44(7–8):1881–1900
- Mishra AK, Singh VP (2010) A review of drought concepts. *J Hydrol* 391(1–2):202–216
- Molteni F (2003) Atmospheric simulations using a GCM with simplified physical parametrizations. I: model climatology and variability in multi-decadal experiments. *Clim Dyn* 20(2):175–191
- Naik M, Abiodun BJ (2016) Potential impacts of forestation on future climate change in Southern Africa. *Int J Climatol* 36(14):4560–4576
- Nicholson SE (2000) The nature of rainfall variability over Africa on time scales of decades to millenia. *Global Planet Change* 26(1–3):137–158
- Nicholson SE, Entekhabi D (1987) Rainfall variability in equatorial and southern Africa: relationships with sea surface temperatures along the southwestern coast of Africa. *J Clim Appl Meteorol* 26(5):561–578
- Nicholson SE, Kim J (1997) The relationship of the El Niño–Southern oscillation to African rainfall. *Int J Climatol* 17(2):117–135
- Nicholson SE, Selato JC (2000) The influence of La Niña on African rainfall. *Int J Climatol* 20(14):1761–1776
- Reason CJC (2001) Subtropical Indian Ocean SST dipole events and southern African rainfall. *Geophys Res Lett* 28(11):2225–2227
- Reason CJC, Jagadheesha D (2005) A model investigation of recent ENSO impacts over southern Africa. *Meteorol Atmos Phys* 89(1–4):181–205
- Reason CJC, Allan RJ, Lindesay JA, Ansell TJ (2000) ENSO and climatic signals across the Indian Ocean basin in the global context: part I, Interannual composite patterns. *Int J Climatol* 20(11):1285–1327
- Rouault M, Richard Y (2005) Intensity and spatial extent of droughts in southern Africa. *Geophys Res Lett* 32(15):L15702
- Rouault M, Florenchie P, Fauchereau N, Reason CJ (2003) South East tropical Atlantic warm events and southern African rainfall. *Geophys Res Lett* 30(5):1505
- Saji NH, Goswami BN, Vinayachandran PN, Yamagata T (1999) A dipole mode in the tropical Indian Ocean. *Nature* 401(6751):360
- Shannon LV, Boyd AJ, Brundrit GB, Taunton-Clark J (1986) On the existence of an El Niño-type phenomenon in the Benguela system. *J Mar Res* 44(3):495–520
- Shongwe ME, Van Oldenborgh GJ, Van Den Hurk BJJM, De Boer B, Coelho CAS, Van Aalst MK (2009) Projected changes in mean and extreme precipitation in Africa under global warming. Part I: Southern Africa. *J Clim* 22(13):3819–3837
- Stone DA, Risser MD, Angéilil OM, Wehner MF, Cholia S, Keen N, Krishnan H, O’Brien TA, Collins WD (2018) A basis set for exploration of sensitivity to prescribed ocean conditions for estimating human contributions to extreme weather in CAM5. 1-1degree. *Weather Clim Extremes* 19:10–19
- Stone DA, Christidis N, Folland C, Perkins-Kirkpatrick S, Perlwitz J, Shiogama H, Wehner MF, Wolski P, Cholia S, Krishnan H, Murray D, Angéilil O, Beyerle U, Ciavarella A, Dittus A, Quan X, Tadross M (2019) Experiment design of the international CLIVAR C20C + detection and attribution project. *Weather Clim Extremes* 24:100206
- Strengers BJ, Müller C, Schaeffer M, Haarsma RJ, Severijns C, Gerten D, Schaphoff S, van den Houdt R, Oostenrijk R (2010) Assessing 20th century climate–vegetation feedbacks of land-use change and natural vegetation dynamics in a fully coupled vegetation–climate model. *Int J Climatol* 30(13):2055–2065
- Trambauer P, Maskey S, Werner M, Pappenberger F, Van Beek LPH, Uhlenbrook S (2014) Identification and simulation of space–time variability of past hydrological drought events in the Limpopo River basin, southern Africa. *Hydrol Earth Syst Sci* 18(8):2925–2942
- Tyson PD, Preston-Whyte RA (2000) *Weather and climate of Southern Africa*. Oxford University Press, Oxford
- Ujenezela EL, Abiodun BJ (2015) Drought regimes in Southern Africa and how well GCMs simulate them. *Clim Dyn* 44(5–6):1595–1609
- Vicente-Serrano SM, Beguería S, López-Moreno JI (2010) A multiscale drought index sensitive to global warming: the standardized precipitation evapotranspiration index. *J Clim* 23(7):1696–1718
- Wang G, Eltahir EA (2000a) Ecosystem dynamics and the Sahel drought. *Geophys Res Lett* 27(6):795–798
- Wang G, Eltahir EA (2000b) Role of vegetation dynamics in enhancing the low-frequency variability of the Sahel rainfall. *Water Resour Res* 36(4):1013–1021
- Wilhite DA (ed) (2000) *Drought as a natural hazard: concepts and definitions*, Chap 1. In: *Drought: A Global Assessment*, vol I. Drought Mitigation Center Faculty Publications, Routledge, London, pp 3–18
- Wilson AB, Bromwich DH, Hines KM, Wang SH (2014) El Niño flavors and their simulated impacts on atmospheric circulation in the high southern latitudes. *J Clim* 27(23):8934–8955
- Yadav RK, Yoo JH, Kucharski F, Abid MA (2010) Why is ENSO influencing northwest India winter precipitation in recent decades? *J Clim* 23(8):1979–1993
- Yuan C, Tozuka T, Landman WA, Yamagata T (2014) Dynamical seasonal prediction of Southern African summer precipitation. *Clim Dyn* 42(11–12):3357–3374
- Zeng N, Yoon J (2009) Expansion of the world’s deserts due to vegetation–albedo feedback under global warming. *Geophys Res Lett*. <https://doi.org/10.1029/2009GL039699>
- Zeng N, Neelin JD, Lau KM, Tucker CJ (1999) Enhancement of interdecadal climate variability in the Sahel by vegetation interaction. *Science* 286(5444):1537–1540

**Publisher’s Note** Springer Nature remains neutral with regard to jurisdictional claims in published maps and institutional affiliations.